Correspondence to:
L. Mei,
mei@iup.physik.uni-bremen.de

A Critical Evaluation of Deep Blue Algorithm Derived AVHRR Aerosol Product Over China

Linlu Mei[1] [ID], Chuanxu Zhao[1], Gerrit de Leeuw[2,3] [ID], John P. Burrows[1] [ID], Vladimir Rozanov[1], HuiZheng Che[4], Marco Vountas[1] [ID], Annette Ladstätter-Weißenmayer[1], and Xiaoye Zhang[4]

[1]Institute of Environmental Physics, University of Bremen, Bremen, Germany, [2]Climate Research Unit, Finnish Meteorological Institute, Helsinki, Finland, [3]School of Atmospheric Physics, Nanjing University of Information Science and Technology, Nanjing, China, [4]Key Laboratory of Atmospheric Chemistry, Chinese Academy of Meteorological Sciences, CMA, Beijing, China

Abstract The Deep Blue (DB) aerosol retrieval algorithm has recently been applied to Advanced Very High Resolution Radiometer (AVHRR) data to produce a first version (V001) of a global aerosol optical thickness (AOT) data set. In this paper, we critically evaluate these AVHRR AOT data over China by comparison with ground-based reference data from China Aerosol Remote Sensing Network for the period 2006–2011. The evaluation considers the impact of the surface (type and reflectance) and the aerosol properties (aerosol loading, aerosol absorption) on the quality of the retrieved AOT. We also compare the AVHRR-retrieved AOT with that from Moderate Resolution Imaging Spectroradiometer over major aerosol source regions in China. We further consider seasonal variations and find, in general, a good agreement between AVHRR AOT and the reference data sets. The AVHRR retrieval algorithm performs well over dark vegetated surfaces, but over bright surfaces (e.g., desert regions) the results are less good. The AVHRR algorithm underestimates the AOT, with 32.1% of the values lower than the estimated error envelope of $\pm 0.05 \pm 0.25\tau$. In particular over the desert, the AVHRR-retrieved AOT is frequently underestimated and for AOT ≤ 0.6 the values are on average 0.05 too low due to the pixel filtering, and dust storms are missed. The comparison of the AVHRR AOT with MODIS collection 6 and CARSNET data indicates that improvements are needed for, for example, AVHRR calibration and cloud/aerosol flagging. The analysis presented in this paper contributes to a better understanding of the AVHRR AOT product over China.

1. Introduction

Satellite observations of the radiance at the top of the atmosphere (TOA) are used to retrieve the aerosol optical thickness (AOT), which is widely used for regional air quality monitoring and global climate change evaluation (Kaufman et al., 2002). The design of AOT retrieval algorithms strongly depends on instrument characteristics and vary by the way that effects of surface and atmospheric contributions to the measured TOA reflectance are accounted for (de Leeuw et al., 2018; Hsu et al., 2004; Hsu et al., 2013; Kaufman et al., 1997; Levy et al., 2013; Mei, Xue, de Leeuw, et al., 2012; Mei, Xue, Xu, et al., 2012; Popp et al., 2016; Sayer et al., 2012). Long-term AOT data sets allow for the analysis of the temporal evolution of the AOT and the determination of trends, which are important for understanding of the effects of aerosol particles and their precursors, of both natural and anthropogenic origin, on air quality and on processes affecting the Earth's climate through direct and indirect effects, as well as the efficiency of measures to improve air quality. One challenge for the construction of a consistent long-term AOT data set from satellite observations is the limited lifetime of satellite-based instruments, of the order of a decade (Mei et al., 2018). Hence, to create a multidecadal data record, multiple sequential instruments are needed which, however, may create issues due to differences in instrument characteristics such as viewing geometry, swath and spatial resolution, spectral bands and their widths, polarization, and calibration uncertainties and instrument degradation, which impact data consistency (Li et al., 2009). Such issues have been addressed in several studies, such as for the combination of Moderate Resolution Imaging Spectroradiometer (MODIS) and Visible Infrared Imaging Radiometer Suite data sets to create an aerosol record of nineteen years till today (Levy et al., 2015; Sayer et al., 2015). Also, as part of the European Space Agency (ESA) Climate Change Initiative (CCI; Hollmann et al., 2013) project Aerosol_cci, the combination of ATSR2 (Along Track Scanning Radiometer 2) and AATSR (Advanced Along Track Scanning Radiometer) has been proposed to construct an aerosol data

record of 17 years (de Leeuw et al., 2018; Popp et al., 2016). Three different algorithms have been applied to the same ATSR L1b data, providing slightly different results and performance records, although none of these three algorithms appears to outperform the other two everywhere (de Leeuw et al., 2015). The consistency between the ATSR-2 and AATSR AOT data sets over China, retrieved using the FMI dual view aerosol retrieval algorithm ADV (Kolmonen et al., 2016; Sogacheva et al., 2017) v2.31, is discussed in Sogacheva et al. (2018) and shows that the combination of data produced with the same algorithm applied to these two similar sensors does provide a consistent data set. On the other hand, a substantial offset occurs between AOT retrieved from MODIS-Terra and the ADV-retrieved ATSR AOT, with MODIS-Terra AOT about 0.15 higher (de Leeuw et al., 2018; Sogacheva et al., 2018).

Extension of the global AOT on a multidecadal time scale is important to improve our understanding of aerosol effects and the influence on aerosol properties of the changing environment (meteorological, climate) and anthropogenic factors (industrial development, population change and migration, mitigation, etc.) on yearly to decadal time scales (Mei et al., 2017a). To achieve this, the use of AVHRR for AOT retrieval could provide a unique time series starting in the early 1980s and the AVHRR Level1 data are available for the whole period starting from 1980s. Retrieving aerosol properties from AVHRR data is challenging because of the band-setting limitation (Mishchenko et al., 2007); that is, only two spectral bands are available, at 0.63 and 0.87 μm, as opposed to the shorter wavelengths which are usually applied for aerosol retrieval and are more sensitive to smaller aerosol particles than these longer wavelengths. Furthermore, the bandwidth of the 0.87μm channel is very wide (0.725 –1.1 μm) and can be contaminated by water vapor absorption (Hsu et al., 2017). The AOT varies with wavelength (λ) as $\lambda^{-\alpha}$, where the value of α depends on the aerosol size distribution and is typically in the range of 0 for coarse-mode dominated aerosols to >1 for fine-mode dominated aerosol types. Hence, the use of a broadband channel introduces a type-dependent uncertainty.

Until recently, AVHRR aerosol retrieval algorithms mainly focused on the atmosphere over the ocean (Geogdzhayev et al., 2002; Mishchenko et al., 2007), because of its very low and spectrally flat surface reflectance (Hauser et al., 2005). This was demonstrated with three algorithms, including the Global Aerosol Climatology Project (GACP) (Geogdzhayev & Mishchenko, 2015), the NOAA aerosol climate data record (CDR) (Zhao et al., 2016), and the Satellite Ocean Aerosol Retrieval (SOAR) algorithm (Sayer et al., 2012). Attempts for aerosol retrieval over land using AVHRR data were made by, for instance, Hauser et al. (2005), Takemata et al. (2006), and Riffler et al. (2010). Validation of the AOT retrieved in these studies show different correlations with AERONET data (between 0.3 and 0.7). Mei et al. (2014) developed a new aerosol retrieval algorithm for application to AVHRR data using the assumptions that (1) the AOT of fine-mode aerosols is negligible at 3.75 μm and (2) empirical relationships between the land surface reflectances in the AVHRR 0.63 and 3.75 μm channels can be derived as a function of surface type (or NDVI). The Mei et al. (2014) AVHRR algorithm is similar to the MODIS Dark Target (DT) algorithm (Levy et al., 2013), except for using the 3.75 μm channel instead of the 2.1 μm channel to estimate the surface reflectance in the visible channels. The Mei et al. (2014) AVHRR AOT retrieval algorithm was further developed and then applied to retrieve AOT time series over North China and central Europe from 1983 to 2015 (Xue et al., 2017). Gao et al. (2016) proposed a neutral-network based method for the retrieval of AOT from AVHRR data over China. However, until recently no algorithm has been applied to the full AVHRR record to produce a global publicly available aerosol data product (Sayer et al., 2017). This gap was filled by the modified version of the Deep Blue algorithm which was applied to the AVHRR instrument as described by Hsu et al. (2017) and Sayer et al. (2017). The validation of this AVHRR AOT data set, using sun photometer data from the China Aerosol Remote Sensing Network (CARSNET; Che et al., 2009, 2015) as reference data (see below), is presented in this paper. In this study, we use AVHRR-DB derived version 1 (V001) AOT data.

Newly developed satellite-derived global aerosol products need to be thoroughly validated versus independent reference data, such as those provided by the AERONET Sun photometer network (https://aeronet.gsfc.nasa.gov/; Holben et al., 1998), which provides long-term and accurate AOT measurements for specific locations. The difficulties associated with the validation of satellite aerosol products, including the required spatial, temporal, and spectral collocation of satellite aerosol products with reference data, has been described in detail in Mei, Xue, de Leeuw, et al. (2012). The most widely accepted match-up criteria were proposed by Ichoku et al. (2002). These authors match the AOT spatial sampling of an instantaneous satellite observation to the temporal sampling of a local Sun photometer measurement; that is, the satellite

observations are averaged in a $50 \times 50\text{-km}^2$ square spatial window which matches 1 hr of temporal Sun photometer data (±30 min around the satellite overpass time). This method is also applied in the current study.

The initial validation of the AVHRR-retrieved AOT using AERONET data shows that the expected error confidence interval envelope for the initial AVHRR AOT product is around $\pm(0.03 + 15\%)$ over ocean and $\pm(0.05 + 25\%)$ over land (Hsu et al., 2017; Sayer et al., 2017). These numbers apply to the global data set. As reported by Sayer et al. (2017), the accuracy of the AVHRR-DB-retrieved AOT over land tends to be underestimated in high-AOT conditions due to both algorithmic assumptions and sensor calibration issues. Over China, however, due to the limited and temporally/spatially unbalanced distribution of AERONET observations, the understanding of satellite aerosol products is not as good as for other areas such as, for instance, over the United States and Europe (Mei, Xue, de Leeuw, et al., 2012). On the other hand, another independent and high quality in situ aerosol data set over China is available from CARSNET (Che et al., 2009, 2015). CARSNET is a ground-based Sun photometer network for monitoring aerosol optical properties over China, and it uses the same types of instruments and processing algorithms as AERONET. CARSNET data are available on request for the validation and better understanding of the satellite-derived aerosol products (contact Dr. Huizheng Che for more information).

The goal of this study is to perform the first critical evaluation for the new AVHRR AOT products over China, using CARSNET data, and provide AOT error characteristics. The study encompasses the years 2006–2011, that is, when both CARSNET and AVHRR/NOAA18 data are available. The evaluation of the global AVHRR-derived AOT using AERONET is presented in Sayer et al. (2017) and therefore AERONET data are not included in this study. The results of this study provide knowledge on the quality of the initial AVHRR AOT product in a range of surface and aerosol conditions in China to the Deep Blue team for possible improvement of the algorithm for these conditions resulting in future processing with improved quality, controlled uncertainty, and sufficient spatial resolution. Section 2 describes the Deep Blue aerosol retrieval algorithm; because the validation presented in this paper is limited to land surfaces, the SOAR algorithm (Sayer et al., 2012) is not included. Section 3 presents the auxiliary data products used in the validation. Section 4 describes the general validation methodology. Section 5 provides an overall validation of the AVHRR-DB AOT over China, including a test of spatial-temporal collocation between AVHRR and CARSNET data. A comparison between AVHRR and MODIS AOT is also presented in section 5. Section 6 further analyzes the AOT bias with respect to different surface and atmospheric conditions. Section 7 provides a brief summary.

2. Overview of the Deep Blue AVHRR Algorithm

The validation in this paper focuses on AVHRR-retrieved AOT product version 1 (V001) over land retrieved with the DB algorithm with a resolution of approximately 8.8×8.8 km. Attempt proposed new calibration method to create the long-term record of AVHRR TOA reflectance (Song et al., 2018). The calibration status of AVHRR and other instruments were discussed during the workshop on Radiometric Calibration for European Optical Missions (https://earth.esa.int/web/sppa/meetings-workshops/expert-meetings/workshop-on-radiometric-calibration-for-european-optical-missions). The AVHRR3 (https://wdc.dlr.de/sensors/avhrr3/) instrument flies on board MetOp-A, B, and C. The workshop results show the good performance of the AVHRR sensors on the MetOp satellites; that is, for MetOp-A, the correlation between channel 1 (0.63 µm) and the same channel on the Global Ozone Monitoring Experiment is higher than 0.99 (https://earth.esa.int/documents/700255/3194632/J%2B%C3%82rgAckermann_AVHRR+Operational+Calibration.pdf/bff6d2ec-86c6-4af2-b9a0-e1f0cc0f6f8c, last access 14 March 2019). In this paper, we do not differentiate between the small differences in wavelengths between AVHRR instruments (all are indicated at 0.63 µm). Specifically, central wavelengths for band1 of NOAA11, NOAA14, and NOAA18 are 0.636, 0.636, and 0.633 µm, respectively.

The AVHRR-DB algorithm has been described in detail by Hsu et al. (2017). Major differences between AVHRR-DB and MODIS-DB for cloud screening and various other algorithm constraints are due to the band-setting and well-known calibration issues (there is no onboard solar band calibration for AVHRR) of the AVHRR instrument as compared to the SeaWiFS, MODIS, and Visible Infrared Imaging Radiometer Suite DB algorithms.

The AVHRR-DB algorithm is significantly different from the original DB algorithm developed for MODIS (Hsu et al., 2013) due to the difference in available wavelength bands. Hsu et al. (2013) developed the DB algorithm for bright surfaces taking advantage of the fact that bright surfaces are much darker in the blue spectral region (0.412 μm) than at longer wavelengths (e.g., 0.63 μm). As described in detail in Hsu et al. (2017), the AVHRR-DB algorithm uses a surface reflectance data base at 0.63 μm over urban, dry, and transitional land surfaces, which was constructed at 0.1^o resolution using a minimum reflectivity approach combined with information on the NDVI. Over vegetated surfaces a maximum NDVI (in 30 days) approach was applied to calculate the 0.63-μm reflectance from the Raleigh-corrected reflectance in the 0.85-μm band, and after atmospheric correction to remove residual aerosol effects in the minimum reflectivity approach. Over very bright surfaces, the surface reflectance at 0.63 μm may reach the so-called critical surface reflectance, where the surface reflectance determines the TOA reflectance irrespective of AOT (Fraser and Kaufman, 1985) and thus DB does not provide a retrieval over those very bright surfaces (e.g., snow and ice, some deserts). Following Hsu et al. (2017), in arid regions in China the 0.63-μm surface reflectances are less than the critical value.

Due to the lack of both a blue channel and a 1.38-μm cirrus channel for AVHRR, the previous MODIS cloud screening module has been modified in the AVHRR-DB algorithm to account for the band difference (Hsu et al., 2017). The AVHRR-DB cloud screening is a threshold-based algorithm, with empirical thresholds adapted from the MODIS-DB implementation for AVHRR, which includes (1) a spatial variability test on the TOA reflectance at 0.63 μm within a 3×3 pixel spatial window, (2) a dynamic range test of the surface reflectance at 0.63 μm depending on surface types, (3) checks on brightness temperature at 11 μm, and (4) brightness temperature difference between 11 and 12 μm, and (5) a heavy dust flag by checking on brightness temperature difference between 11 and 12 μm. Details can be found in Hsu et al. (2017).

The regional and seasonal aerosol typing in the DB AVHRR algorithm is, in general, consistent with that in the previous MODIS and SeaWiFS DB algorithms (cf. Hsu et al. (2004, 2013) for details), with adaption to AVHRR wavelengths (Hsu et al., 2017; Sayer et al., 2017). Aerosol typing in DB is based on a maximum likelihood method for predefined aerosol microphysical properties. AVHRR AOT is directly retrieved from AVHRR measurements using the 0.63-μm channel. AOT at 0.55 μm is obtained by extrapolation using an Ångström exponent climatology created from the AERONET data record as described by Hsu et al. (2017). Thus additional "retrieval error" may be introduced during the extrapolation. In summary, uncertainties in the AVHRR Deep Blue AOT product may be introduced by (1) usage of a climatology of seasonal and regional aerosol types, (2) using a single channel in the retrieval (tuning by the wavelength-dependent characteristics is not possible), (3) extrapolation based on Ångström exponent climatology, (4) deviation from surface assumption, and (5) cloud contamination.

3. Data

3.1. CARSNET

CARSNET complements the limited number of AERONET sites in China (which are mainly located in SE China) with more than 50 stations across the whole country (see the map in Figure 1). The instruments used in CARSNET are CIMEL CE-318 Sun photometers, similar (but not exact) to those used in AERONET (Che et al., 2009, 2015). CARSNET is not part of AERONET, but uses similar procedures and protocols. Differences between CARSNET and AERONET have been reported by Che et al. (2015), including the use of different types of CIMEL instruments in CARSNET. The CARSNET Sun photometers are calibrated every year to ensure their proper performance and the quality of the measurements (Che et al., 2009). The CARSNET data used in this paper cover the period 2006–2011. Figure 1 shows the locations of the CARSNET and AERONET sites in China, overlaid over a surface types (see legend) map generated by the ESA land-cover CCI project (Bontemps et al., 2011; see section 3.4). An overview of the CARSNET data (including locations of the stations) has been presented by Che et al. (2015).

3.2. ESA Land Cover Data Set

The quality of satellite-retrieved aerosol products depends on the effective separation of the surface and atmospheric contributions to the measured TOA reflectance. As discussed above, the AVHRR-DB algorithm utilizes a surface reflectance data base constructed using a minimum reflectivity approach combined with
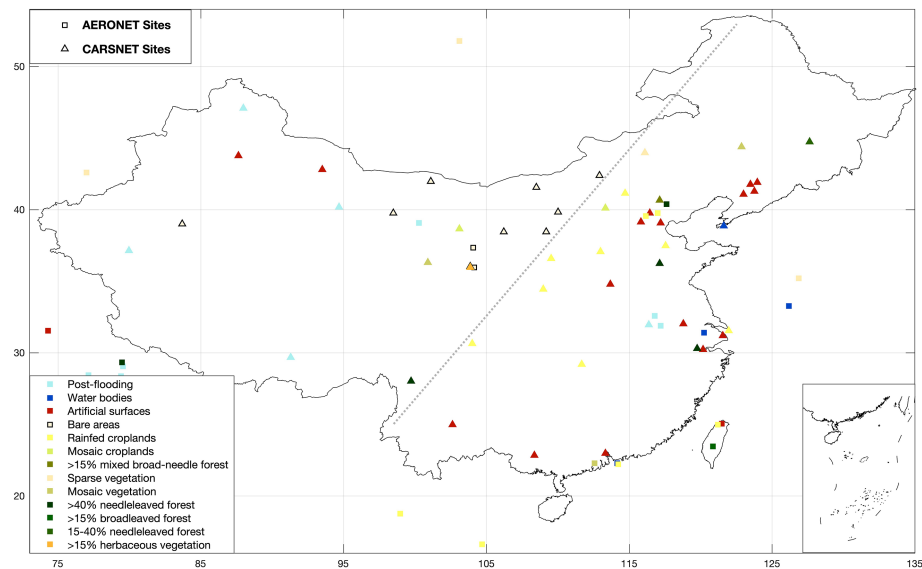
Figure 1. The distribution of CARSNET across China overlaid over the surface types maps generated by land-cover CCI project (Bontemps et al., 2011).

information on the NDVI. For the evaluation of the effect of the surface reflectance on the AOT retrieval results, the latter are compared with AOT reference data from CARSNET over different surface types. The information on surface type used in this paper is obtained from the land cover data set generated by the ESA Land-Cover (LC) Climate Change Initiative (cci) project. This data set includes the 300-m annual global land cover time series from 1992 to 2015. The ESA cci program includes 12 subprojects as described in Hollmann et al. (2013) (see also http://cci.esa.int/). The LC-cci project aims to generate the land cover Essential Climate Variables. The overall LC-cci objective is to critically revisit all participating algorithms required for the generation of a global land product, using moderate spatial resolution (Medium Resolution Imaging Spectrometer full resolution and reduced resolution, SPOT VEGETATION; Landsat-8, Sentinels, ALOS-2, PROBA-V) and ESA SAR sensors, in the light of Global Climate Observing System requirements, and to design and demonstrate a prototype system delivering in a consistent way, over years and from various Earth Observation (EO) instruments, global land cover information matching the needs of key users belonging to the climate change community (https://www.esa-landcover-cci.org/?q= overview). The Medium Resolution Imaging Spectrometer 300-m land cover surface type is used in this study. Details can be found in Bontemps et al. (2011) (http://due.esrin.esa.int/files/GLOBCOVER2009_ Validation_Report_2.2.pdf). The land cover products have been widely used in different study areas, such as the effect of vegetation change on Earth's surface energy balance (Duveiller et al., 2018), and these user cases demonstrate the good quality of the cci data set. Taking the surface variety into account, in this paper, the most frequent surface type in a 50×50-km^2 window (the ratio of the number of pixels of given surface type to the total number of pixels) is selected as the surface type for each match-up.

3.3. AVHRR Surface Reflectance

In this paper, the surface reflectance at 0.63 μm obtained from the Long-Term Data Record (LTDR) project is used and collocated with CARSNET to investigate the dependence of satellite aerosol data on surface reflectance. The LTDR project is aimed at producing a validated global land surface climate data record. LTDR provides atmospherically corrected surface reflectance from AVHRR onboard NOAA satellites from 1981 to present. The latest version 5 AVHRR L1B data products were released on 15 August 2017. Validation shows that LTDR AVHRR data agree well with MODIS data and Pathfinder AVHRR Land (PAL) data. The algorithm includes the retrieval of land surface reflectances for Channels 1-3 of AVHRR, the associated NDVI, and corresponding cloud, cloud/shadow, and snow masks. This data set contains gridded daily surface reflectances and brightness temperatures derived from the AVHRR sensors onboard seven NOAA polar orbiting satellites: NOAA-7, -9, -11, -14, -16, -17, and -18. The AVHRR surface reflectance is processed from

the AVHRR Global Area Coverage (GAC) Level 1b data set. AVHRR GAC observations are packaged into data arrays with latitude and longitude dimensions of 3,600 × 7,200 covering the globe at 0.05-degree spatial resolution. Thus, although the aerosol and surface reflectance are produced using data from the same instrument, collocation is needed due to the different gridding.

3.4. ECMWF Single Scattering Albedo

The aerosol absorption is one of the most critical factors affecting the AOT retrieval quality. The currently available aerosol information from CARSNET does not include information such as aerosol single scattering albedo (SSA), a measure for aerosol absorption. Therefore, the SSA simulated by the European Centre for Medium-Range Weather Forecasts (ECMWF) using a chemical model is used to investigate the dependence of AVHRR-retrieved AOT on the aerosol absorption. The ECMWF model computes the optical properties for five different components: sea salt (SS), dust (DU), organic (OM) and black carbon (BC), and sulfate (SU) aerosols, and the SSA is calculated as a weighted column mean by dividing the total aerosol scattering in the column by the columnar aerosol extinction for each of these. The SSAs for each predefined component (SS/DU/OM/BC/SU) are prescribed in a look-up table (LUT) for various wavelengths and relative humidities. The LUT were calculated by an off-line Mie scattering model, based on the assumed size distributions, refractive indices, and hygroscopic growth properties for each component. The ECMWF SSA product (absorbing product) has been used and discussed in Shin et al. (2019) and shows good quality. The validation of black carbon (BC) aerosol in the ECMWF model has been analyzed and validated using AERONET in Shin et al. (2019); further comprehensive validation for SSA is ongoing. The validation results over Beijing and Xianghe show the good agreement between model and AERONET-retrieved BC column-integrated concentrations with a correlation coefficient between 0.6 and 0.8. For intensive error analysis highly accurate reference SSA data are required, and several models show the large variation of SSA and difference with satellite measurements as described in Lacagnina et al. (2015). More information on the assumptions can be found in Technical Memorandum 801 (https://www.ecmwf.int/en/elibrary/17219-implementation-cams-based-aerosol-climatology-ifs) (Personal communication with Dr. Zak Kipling on September 2017).

4. Validation Strategy

Following previous studies (Ichoku et al., 2002; Remer et al., 2002; Levy et al., 2013; Sayer et al., 2013), a spatial-temporal matching-up method for the comparison of AVHRR AOT and CARSNET AOT is used in this paper. The main idea is that the averages of satellite-derived aerosol properties in a proper spatial window are comparable to their ground-based equivalent averaged in a temporal window corresponding to the average aerosol travel time across the spatial window (Mei, Xue, de Leeuw, et al., 2012; Mei, Xue, Xu, et al., 2012). The first question which needs to be addressed is the choice of a proper spatial-temporal window which is committed to an optimum balance between correlation quality and sample size (Martins et al., 2017; Virtanen et al., 2018). In this paper, we tested nine combinations with three spatial (radius = 12.5, 25, and 50 km centered around the Sun photometer site) and three temporal (time = ±30, ±60 and ±90 min, indicating the time range covering the satellite overpass time) windows. Additionally, we require at least two CARSNET observations in the temporal window and 20% valid retrievals in the spatial window centered over a CARSNET site Mei, Xue, de Leeuw, et al. (2012). The sample sizes are expected to increase with the increase of both spatial and temporal windows. Meanwhile, the spatially averaged AOT from satellite retrievals and temporally averaged AOT from CARSNET observations may not be representative due to large spatial and temporal variabilities. The best situation is that aerosol properties do not change over both the spatial and temporal intervals.

CARSNET does not provide AOT at 0.55 μm, and thus, data are interpolated to 0.55 μm using the Ångström exponent α, defined as

$$\alpha = \frac{\ln(\tau_1/\tau_2)}{\ln(\lambda_2/\lambda_1)} \tag{1}$$

where τ_1 and τ_2 are the AOT at wavelengths λ_1 and λ_2. In this work, λ_1 and λ_2 are 0.44 and 0.87 μm. Negligible uncertainty is introduced through this spectral interpolation (Sayer et al., 2013).

Figure 2 shows scatter density plots of the AVHRR AOT at 0.55 μm versus the CARSNET AOT at 0.55 μm, for a combination of spatial (25 km) and temporal (30 min) windows. Table 1 shows the major statistical
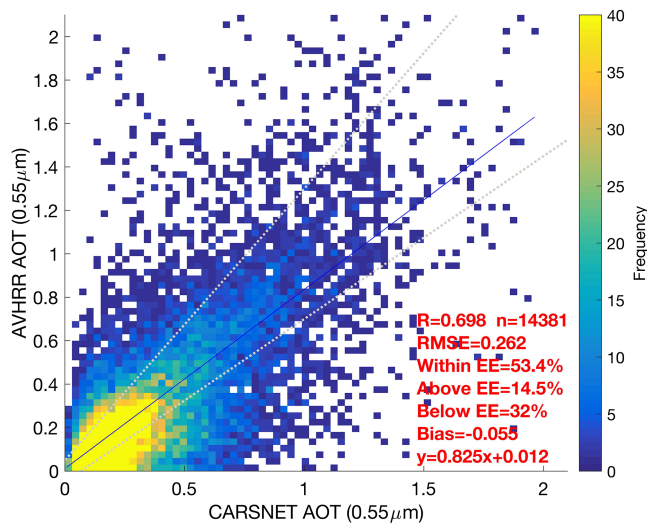
Figure 2. Scatter density plot of AVHRR AOT (0.55 μm) and CARSNET AOT (0.55 μm) for spatial (25 km) and temporal (30 min) windows.

parameters describing the comparison (number of match-ups, Pearson correlation coefficients, RMSE/bias). The data in Figure 2 and Table 1 show the large increase of the match-up numbers with the increase of spatial and/or temporal windows, as expected. About 50% (11,038 versus 15,915) increment of match-ups can be found for ±30 min/±12.5 km compared to ±60 min/±25 km. Other statistical parameters such as the RMSEs and biases are also different, they are (0.242/−0.053) and (0.272/−0.058), respectively. The correlation coefficients are very similar between ±12.5 and ±25 km with decreases of 5–10% for spatial window of ±50 km compared to ±12.5 km. One interesting feature is that the minimal bias (not absolute) occurs for the longest temporal windows, indicating the mitigation of the random uncertainty from AVHRR. The minimal RMSE (0.262) occurs for the temporal window of ±30 min. Thus, a spatial radius of ±25 km for satellite data and a temporal window of ±30 min for CARSNET data are used, in agreement with previous publications by Levy et al. (2013) and Sayer et al. (2013).

The following statistical parameters are used to evaluate the validation quality. The expected error (EE) envelope, which is widely used for the evaluation of satellite aerosol products, has been defined in this paper as ± (0.05 ± 0.25 AOT) for the AVHRR AOT product over land, following Hsu et al. (2017) and Sayer et al. (2017). The EE envelope includes the absolute (0.05) and relative (0.25) uncertainties of AOT retrievals, which are influenced by parameters such as surface properties, sensor calibration, aerosol models, cloud contamination, and empirical thresholds (Levy et al., 2010; Martins et al., 2017). Additionally, the root-mean-square errors (RMSE) and mean bias are calculated:

$$RMSE = \sqrt{\frac{1}{n}\sum_{i=1}^{n}\left(\tau_{satellite} - \tau_{ground}\right)^2} \qquad (2)$$

$$Bias = \frac{1}{n}\sum_{i=1}^{n}\left(\tau_{satellite} - \tau_{ground}\right) \qquad (3)$$

where $\tau_{satellite}$ and τ_{ground} are the satellite-derived and ground-based observed AOT. n is the number of match-up pairs used in the validation.

5. Overall Comparison

The aerosol data used in this paper were retrieved from the AVHRR sensor, flying on the NOAA18 satellite with a local solar equator crossing time of ~2:00 pm, which is close to the MODIS/Aqua equator crossing time (~1:30 pm). Thus, MODIS/Aqua retrieved AOT data (C6.1), downloaded from (https://ladsweb.modaps.eosdis.nasa.gov/search/), is used for comparison. The validation of MODIS AOT with respect to the effects of surface types, aerosol loading, and aerosol absorption has been discussed in detail by Liu et al. (2019). In order to have an overview of the AVHRR AOT spatial distribution over China, seasonal averages of the AOT retrieved from AVHRR and MODIS/Aqua over China during the years 2006–2011 are shown in Figure 3, for winter (DJF), spring (MAM), summer (JJA), and autumn (SON) (top to bottom). The third column shows the difference in AOT retrieved from both sensors (AVHRR-MODIS). The differences in the AOT patterns between different seasons are mainly due to variations in both local emissions and meteorological conditions. The spatial distributions of the AVHRR and MODIS retrieved AOT are similar, with high AOT over eastern China and much lower to the west of the Heihe-Tengchong line (https://en.wikipedia.org/wiki/Heihe%E2%80%93Tengchong_Line). About 95% of the Chinese people (1.3 billion) live in the eastern part, where anthropogenic emissions are large and increased until recently due to economic growth. The main aerosol source in the western part is the Taklamakan desert, especially in the spring. The AOT distribution in eastern China follows a pattern similar to that of the population distribution (Sogacheva et al., 2018), and AOT hot spots coincide with the locations of major cities in China, such as China's first-tier cities (Beijing, Shanghai, and the Guangzhou and Shenzhen regions). Due to the large local emissions and

Table 1
*The Statistical Parameters for Difference Collocation Spatial and Temporal Windows for Figure 2*

	$t = 30$ min	$t = 60$ min	$t = 90$ min
$R = 12.5$ km	11,038/0.72/0.242/−0.053	12,035/0.709/0.254/−0.05	12,585/0.706/0.267/−0.048
$R = 25.0$ km	14,381/0.698/0.262/−0.055	15,916/0.693/0.272/−0.058	16,761/0.69/0.279/−0.051
$R = 50.0$ km	16,928/0.655/0.292/−0.051	19,125/0.651/0.301/−0.051	20,398/0.649/0.308/−0.05

Note. Shown are number of data points/Pearson correlation coefficient/RMSE/bias.

atmospheric circulation patterns, high AOT occurs over the North China Plain (NCP) in the NE part, the Yangtze River delta (YRD) in the middle, the Pearl River delta (PRD) in the east, and over the Sichuan/Chongqing area in the SW (the definition of NCP, YRD, PRD are approximately [32°–40°N, 114°–121°E], [28°–34°N, 118°–123° E], [22°–23°N, 112°–115°E]). The formation of aerosol and its impact on the local environment and human health over those regions has been thoroughly investigated during measurement campaigns and international project collocation such as the DRAGON project (Holben et al., 2018).

The seasonal variation of the AOT over China is clearly observed in both the AVHRR and MODIS data. Over the Taklamakan desert high AOT, with values higher than 0.8, is observed during the spring. During the summer the AOT over the Taklamakan desert is about 2 times lower (AOT~0.4) than during the spring, while during autumn and winter the AOT is substantially smaller. Most dust events over this region occur during the spring through early summer with a season-invariant diurnal change of more than ±10% for AOT and ±30% for the Ångström exponent (Wang et al., 2004). This agrees with the conclusions from in situ (Wang et al., 2004), satellite (e.g., Proestakis et al., 2018; Tao et al., 2017) observations as well as model simulations (Gong et al., 2003). The seasonal variations in other regions with high aerosol concentrations, that is, eastern China and Sichuan Basin, are different from those over the Taklamakan desert and they are also different from each other. Over eastern China, the highest AOT is observed in the summer, with values of the order of 0.8, and somewhat lower (about 0.6) in the spring and autumn, and minima in the winter, in good agreement with observations by de Leeuw et al. (2018). Over the Sichuan Basin, the seasonal variation is much smaller, with somewhat higher AOT during the winter and spring and a little smaller during the summer and autumn, confirming the AATSR observations described in de Leeuw et al. (2018) and Liu et al. (2011). The Sichuan basin, especially Chengdu (the capital city of Sichuan), and Chongqing have the most rapid economic growth of all cities in China and Chongqing has the fastest GDP (gross domestic product, a measure for economic activity) growth (9.5%) in China. Chengdu and Chongqing rank fifth and ninth of GPD in China. However, the pollution over these regions is trapped in the Sichuan basin which is surrounded by mountains, including the Tibetan Plateau, Daba Mountain, Wu Mountain, Dalou Mountain, and the Yunnan-Guizhou Plateau. This deep mountain-basin topography prevents transport of atmospheric pollutants out of the basin where they accumulate and cause year-round high concentrations of air pollution.

Although the spatial distributions of the AVHRR and MODIS retrieved AOT are similar, their magnitudes are different as shown in the seasonal maps in Figure 3 and especially in the difference maps in the right column which shows differences of up to ±0.3. In general, the AVHRR retrieved AOT is lower over eastern China, by up to more than 0.3, while west of the Heihe-Tengchong line the AVHRR and MODIS/Aqua retrieved AOT are more similar in magnitude, although quite large differences occur, both positive and negative. As shown in de Leeuw et al. (2018), for MODIS/Terra C6, the validation with AERONET shows that MODIS overestimates the AOT over eastern China and over the Tibetan Plateau. Hence, the differences between AVHRR and MODIS may be due to the added overestimation by MODIS and underestimation by AVHRR. The latter will be discussed below. Because the MODIS C6.1 aerosol data used in this study is the merged DTDB AOT product, AOT over vegetated regions (eastern China) is produced by the Dark-Target algorithm while Deep Blue is applied over bright surfaces such as the Taklamakan desert (Sayer et al., 2014). As described in section 2, the fundamental idea of the AVHRR-DB algorithm is similar to that used for MODIS over bright surfaces described in Hsu et al. (2013) and also applied to MODIS C6.1. However, the difference in available wavelength bands for AVHRR and MODIS forced the AVHRR
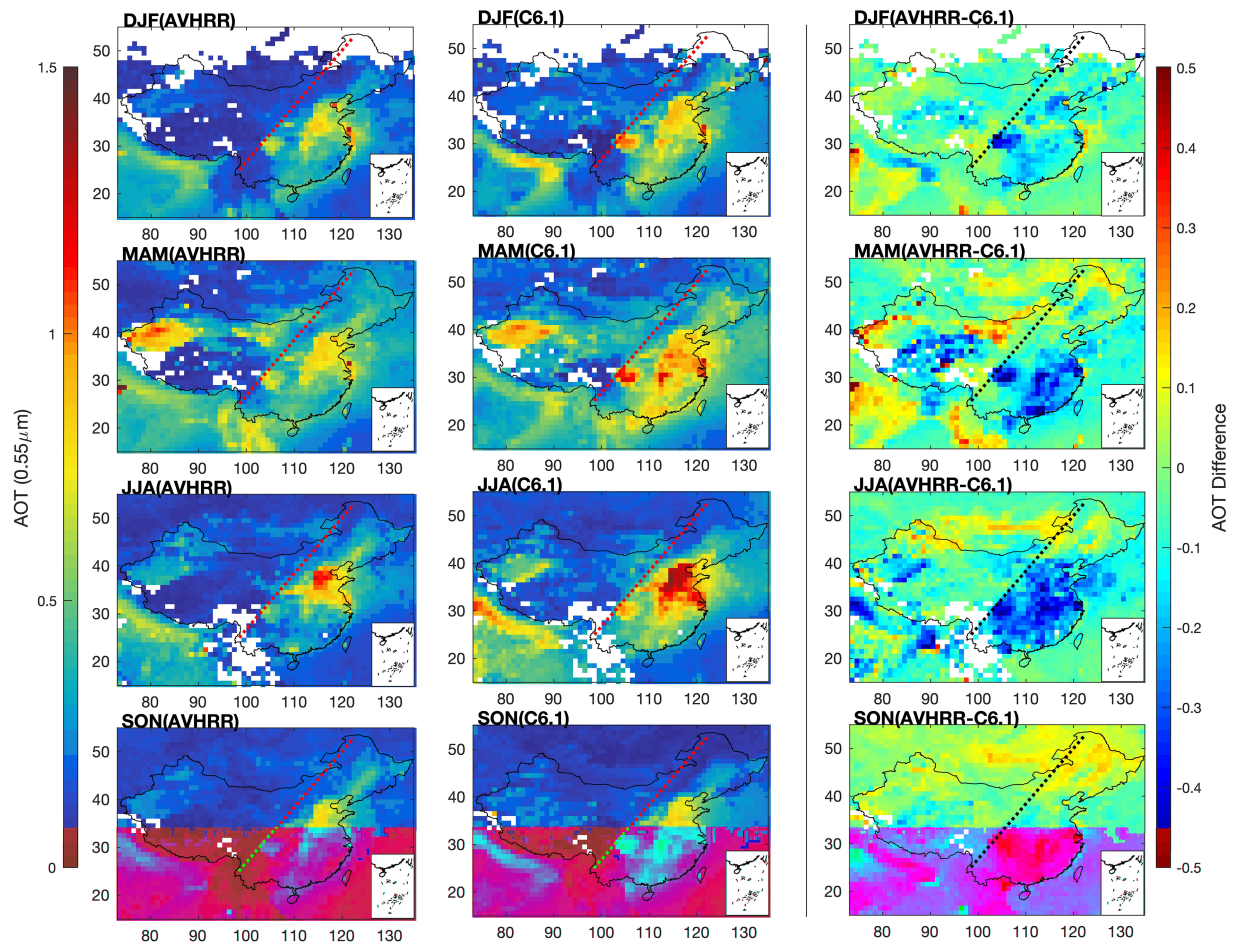
Figure 3. Spatial distributions of the AOT retrieved from AVHRR-DB and MODIS/Aqua-DB (C6.1), averaged over each season during the period 2006–2011, and their differences. (left column) AVHRR. (middle column) MODIS/Aqua. (right column) AVHRR-MODIS. From top to bottom: DJF, MAM, JJA, SON. The dashed line is the Heihe-Tengchong Line (https://en.wikipedia.org/wiki/Heihe%E2%80%93Tengchong_Line, last access 14 March 2019).

retrieval team to apply a different approach for the surface correction (Hsu et al., 2017). For a bright surface like the Taklamakan and Gobi deserts the approaches for AVHRR and MODIS are similar, while also cloud screening and aerosol typing are similar (although updated), which results in the similar AOT over the Taklamakan desert. However, large differences are observed at the edges of Taklamakan desert and in the spring over part of the Gobi desert. Over other regions in China, large differences are observed in most seasons (Figure 3, right column), even though the aerosol retrieval algorithms applied to MODIS and AVHRR are based on similar principles and assumptions, but with the 0.63-μm channel used for AVHRR-DB instead of the 0.412-μm channel used with MODIS-DB which has significant consequences for the most important issues in aerosol retrieval, that is, cloud screening, surface correction, and aerosol model description as described in Hsu et al. (2017). Besides sampling differences between the two instruments (Hsu et al., 2017), the AVHRR/MODIS differences can also be due to the difference in classification of dust events. In MODIS C6 the brightness temperature difference between the 8.6- and 11-μm channels is used to identify the presence of extremely absorbing mineral dust (Hsu et al., 2013). Additionally, a new heavy dust flag developed in Hansell et al. (2007) has been implemented to choose between a three- or two-wavelength retrieval. However, AVHRR does not have such channels and therefore such tests cannot be used and therefore AVHRR may misclassify some dust storms as clouds and thus the aerosol retrieval is not performed and high AOT cases are missed. This results in low AOT in AVHRR-DB compared to MODIS-DB. Xiao et al. (2008) investigated the evolution of dust storms in the Taklimakan desert and its correlation with climatic parameters, showing that sand dust storms in the Taklimakan desert mainly occur in the summer, then in fall, spring, and winter, and the average
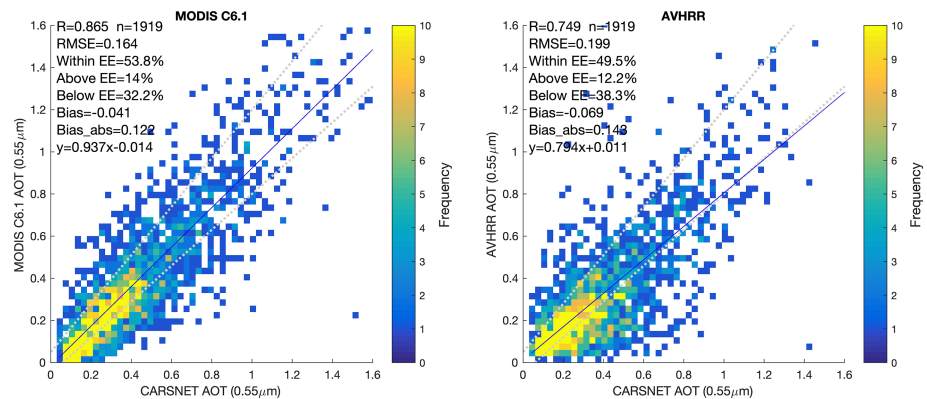
Figure 4. Scatter density plots MODIS C6.1 AOT versus CARSNET AOT and AVHRR-DB AOT versus CARSNET AOT for collocated data points for which all three data sources are available. The white dashed lines indicate the expected error of $\pm 0.05 \pm 0.25\tau$.

fractions are 50.7%, 28.7%, 14.8%, and 5.8% for JJA, SON, MAM, and DJF, respectively. Beside the potential overestimation of surface reflectance, causing underestimation of AOT, overflagging of dust storms in the summer period and uncertainties caused by potential dust aerosol typing could be major reasons for large underestimation of AVHRR-DB AOT over dust regions, as compared to MODIS-DB AOT. Additionally, the impact of calibration issues of AVHRR has been discussed by Sayer et al. (2017).

Large underestimation of AVHRR-DB compared to MODIS can be found in eastern China, where mostly the Dark-Target algorithm is applied (Sayer et al., 2014), indicating that all possible factors (calibration, cloud screening, surface correction, and aerosol assumptions) described in Li et al. (2009) may contribute. Liu et al. (2019) investigated the data quality of the MODIS Dark-Target C6 AOT data over China, including the impact of surface type, aerosol loading and aerosol absorption, and observed slight overestimation with respect to the CARSNET reference AOT data. The results show a large underestimation of MODIS C6 AOT in both coverage (less match-ups with CARSNET) and magnitude in JJA (up to 0.2), then MAM and SON, while in DJF MODIS and CARSNET AOT agreed relatively well. Cloud contamination will in general result in overestimation of the AOT (Martins et al., 2002; Mei et al., 2017b), and hence, the lower AOT values retrieved using AVHRR-DB are more likely due to effects of surface parameterization and aerosol typing then to cloud contamination. Over the Sichuan basin, the AVHRR-DB AOT is also consistently lower than the MODIS C6.1 AOT (Dark-Target retrieval as indicated by the algorithm flag in the MODIS product). The evaluation from Shi et al. (2017) shows that over the Sichuan Basin the MODIS-Dark-Target AOT (C6) slight overestimates the AOT with respect to Sun photometer derived values in Chongqing. However, the DB algorithm substantially underestimates the AOT and this is mainly due to the bias in the surface parameterization. The potential bias of the surface parameterization in AVHRR-DB over vegetated areas can be seen in southern China (e.g., Yunnan and Guangxi), especially during MAM and SON, when the vegetation properties change rapidly. The different patterns over eastern and northern China may be due to differences in aerosol typing. Relatively good agreement between AVHRR-DB and MODIS AOT occurs in DJF, especially over northern China where emission due to heating dominates in the winter. Relatively good agreement is also observed in central China, except in JJA when agricultural biomass burning occurs frequently during late summer (e.g., Anhui, Henan, Jiangsu, and Shandong Provinces; Xue et al., 2017). Due to the limited information content of AVHRR, the simplified aerosol type description (size distribution and refractive index) used to model the aerosol optical properties in the retrieval algorithm, lead to large (systematic) errors in high-AOT conditions (as scattering/absorption properties of marine, dust, smoke, continental, or other aerosol types differ; Sayer et al., 2017). The dependence of the quality of AVHRR-DB AOT on surface types, surface reflectance, and aerosol properties will be discussed in more detail in section 4. A quantitative comparison of the differences between AVHRR-DB and MODIS retrievals is presented in Figure 4 where scatter-density plots are shown of collocated satellite and reference AOT data for AVHRR-DB/CARSNET and for MODIS/CARSNET, for cases where all three data sources are available (altogether, 1919 data pairs). MODIS shows better correlation (0.865 versus 0.749) and lower RMSE (0.164 versus 0.199) than
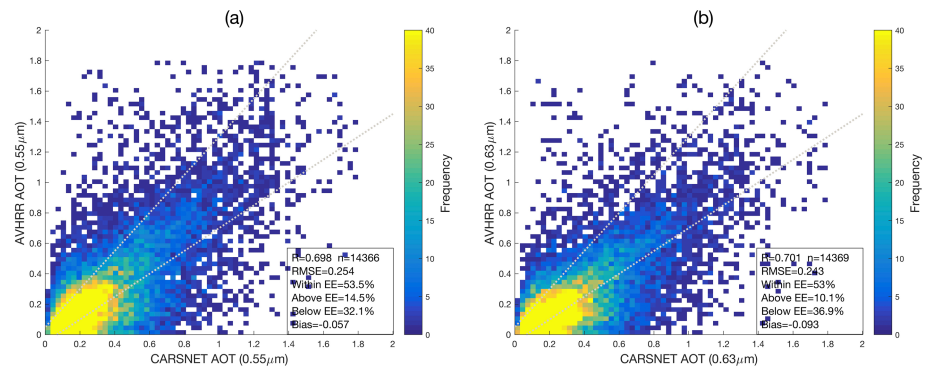
Figure 5. Scatter density plot of AVHRR AOT versus CARSNET AOT at different wavelengths: (left) 0.55 μm and (right) 0.63 μm. The white dashed lines indicate the expected error of ±0.05 ± 0.25τ.

AVHRR-DB. The fraction of data points within EE is about 5% higher for MODIS than for AVHRR. Figure 4 also shows that the AVHRR-DB AOT is biased low while for MODIS-DB the data points are closer to the EE.

For validation, the AVHRR-DB AOT at 0.63 μm is extrapolated to 0.55 μm as described in section 3. In this section the potential uncertainty due to the "extrapolation" is addressed. Figure 5 shows the comparison between AVHRR-DB and CARSNET for both wavelengths, that is, the retrieval wavelengths of 0.63 μm and the extrapolated wavelength of 0.55 μm. A total number of 14,366 match-ups is available for AOT at 0.55 μm and 14,369 for AOT at 0.63 μm (only AOT ≤ 3 is used in the validation, which excludes three match-ups for AOT at 0.55 μm). The total number of match-ups and the representative spatial distribution of CARSNET over China ensure that the validation result is significant. The correlation coefficients of the data sets at both wavelengths with the CARSNET AOT at the same wavelength are similar (0.698 versus 0.701) and also the number of data points within EE is similar for both wavelengths (53.5% versus 53.0%). However, the number of data points below EE is slightly larger at 0.63 μm than at 0.55 μm (36.9% versus 32.1%), whereas the number of data points above EE is somewhat larger at 0.55 μm than at 0.63 μm (14.5% versus 10.1%). Because the "extrapolation" depends purely on the selected aerosol type which prescribes the wavelength dependence of the AOT, the scatterplots should only show clockwise or counterclockwise patterns (change of slope in regression). The slope of the regression line at 0.55 μm (0.80) is significantly larger than that at 0.63 μm (0.7), while the intercepts are almost the same (0.02 versus 0.018). These results show that the extrapolation does not introduce large additional errors for AOT at 0.55 μm. The AVHRR-DB-retrieved AOT has is biased negative; that is, in a statistical sense the AOT is underestimated with respect to the CARSNET reference AOT data. This is illustrated in the histograms in Figure 6 for both wavelengths. The relatively broad histograms show the large deviations of the AVHRR-DB AOT from the CARSNET reference value, both positive
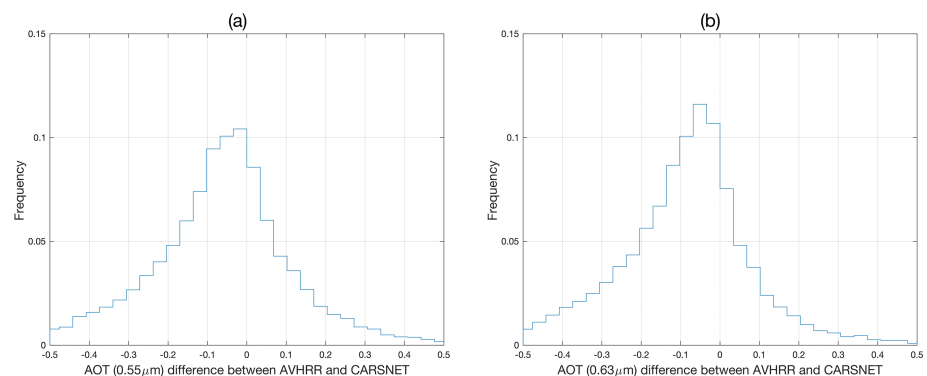

Figure 6. Same as Figure 5 but for histogram
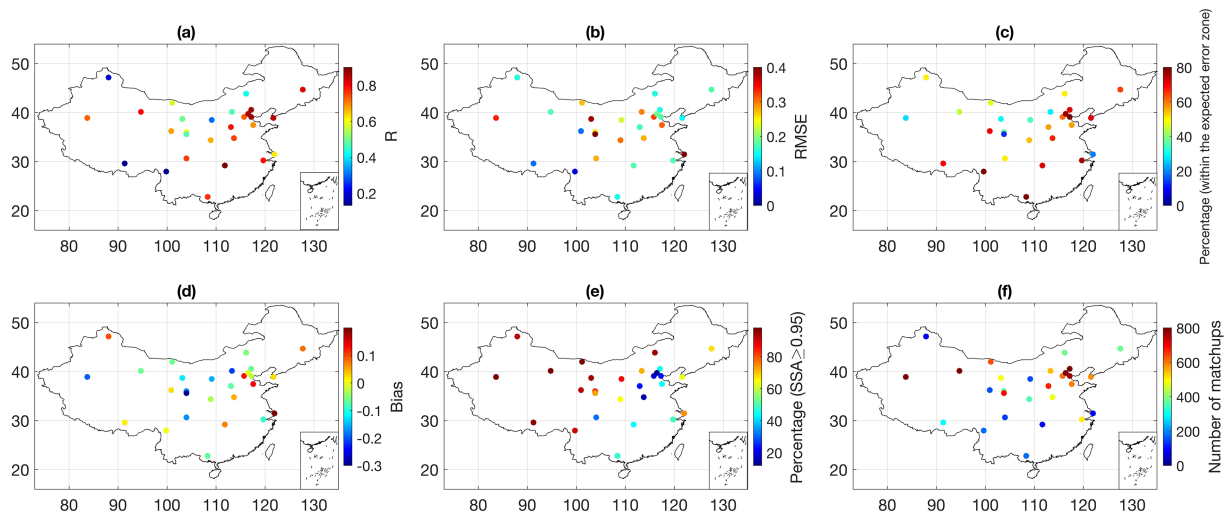
Figure 7. Variation across China of the regression parameters of the AVHRR-retrieved AOT versus CARSNET AOT at individual CARSNET sites: (a) correlation coefficient, (b) RMSE, (c) fraction of data points within EE of $\pm(0.05 + 25\%)$, (d) bias, (e) fraction of data points with SSA > 0.95, and (f) number of match-ups.

and negative, which indicate that improvement for the retrieval can be achieved. The much larger underestimation ($\Delta AOT < -0.2$) than overestimation ($\Delta AOT > 0.2$) also indicates that overfiltering of heavy aerosol episodes has a larger influence on the retrieval results than cloud contamination.

The retrieval quality strongly depends on the geographic location, that is, the surface conditions and the aerosol type. China offers a variety of different surface types and strong variations in aerosol burden and composition, which allows the evaluation of the retrieval data quality by using CARSNET sites at different locations. To this end, the validation strategy discussed in section 3 is followed for each individual site and
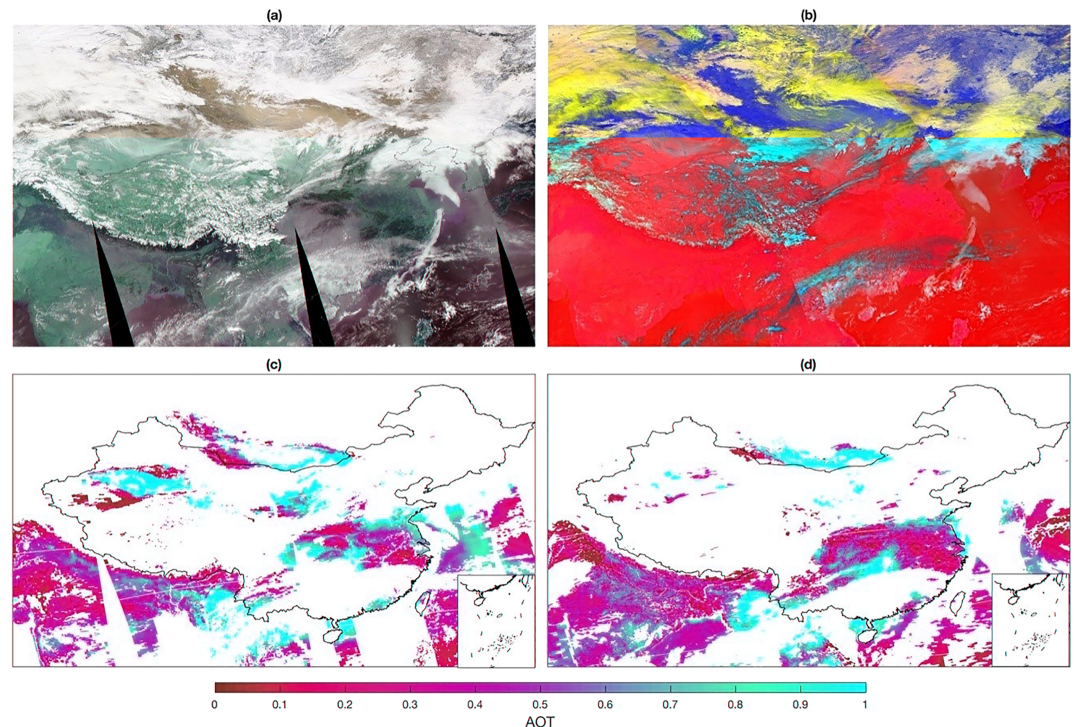
Figure 8. A dust storm event on 19 March 2010. (a) MODIS Aqua true-color image, (b) AVHRR RGB (0.63, 0.87, 10.8 μm) image, (c) MODIS C6.1 AOT at 0.55 μm, and (d) AVHRR AOT at 0.55 μm.

the results are presented in Figure 7: correlation coefficient, RMSE, fraction of data points within EE of ±(0.05 + 25%), bias, fraction of data pints with SSA > 0.95, and the number of match-ups used in the AVHRR validation. More match-ups occur in eastern and northern China than in the south (Figure 7f). Figure 7a shows that correlation coefficients R > 0.7 were obtained for most sites (70%). Figures 7b and 7d show similar spatial distribution patterns for both RMSE and bias in eastern China (longitude >105°), with opposite patterns in western China, indicating consistent positive biases in eastern China (Beijing-Tianjin Metro Region and Yangtze River Delta) and random biases in the west. More than 70% of the sites show a large fraction within EE of 53.5% (the overall fraction within EE for all match-ups as presented in Figure 2). The AOT is mainly underestimated at sites where the absorption is weak. For sites with strong absorption the biases are relatively small, as shown in Figures 7d and 7e. Most match-ups occur over Tazhong (in the Taklimakan desert) and Beijing, both with more than 1,000 match-ups. At the Beijing site, where strong absorption is observed, a large fraction of the data pints is within EE and the bias is low, while at Tazhong the patterns are opposite. These differences in data quality indicate the influence of the surface brightness and aerosol absorption, which will be discussed in section 6.

## 6. Impacts of Factors Linked to Aerosol Retrievals

In this section, the impacts of cloud screening and/or pixel filtering, surface type/surface reflectance, aerosol loading, and aerosol absorption are analyzed to better understand the results presented in the sections above.

6.1. Cloud Screening and Pixel Filtering

Figure 8 shows as an example the AVHRR and MODIS Aqua AOT over China on 19 March 2010 to illustrate the effects of cloud screening and pixel filtering. A heavy dust storm is observed over Mongolia and Inner Mongolia. Figures 8a and 8c show the RGB composites from the MODIS and AVHRR (0.63, 0.87, 10.8 μm) observations. The data show the different swath widths of MODIS and AVHRR (2,330 versus 2,900 km). Clouds and certain surface types are clearly visible in both figures, but due to the channel settings in the AVHRR RGB (following EUMETRAIN, http://www.eumetrain.org/), middle- and low-level clouds are yellow, thick high-level clouds are white, and thin high-level clouds are bluish. This is due to the contribution of reflectivity and brightness temperature. MODIS and AVHRR show very similar patterns and magnitudes, despite the slight differences in observation time. However, the data coverage from the two instruments is somewhat different. AVHRR (Figure 8d) achieves hardly any successful retrieval over northwest China, which is dominated by bright surface and a dust-loaded atmosphere. This may be due to surface reflectance being too high and/or cloud contamination over arid areas (Hsu et al., 2017). The MODIS AOT (Figure 8c) has much better coverage and the AOT pattern is in reasonable agreement with that of the RGB figure. Near Beijing, where a small clear region is surrounded by heavy clouds, AVHRR AOT has slightly better coverage than MODIS. However, the AOT in the few remaining MODIS pixels is much higher than that from AVHRR, indicating the good treatment of cloud adjacency effects (three-dimensional effects; Koren et al., 2007) by excluding pixels adjacent to a pixel identified as cloudy in the AVHRR-DB algorithm. AVHRR also has more successful retrievals than MODIS in the central part of China. However, AVHRR underestimates the AOT for heavy aerosol loading which is well captured by MODIS with sparser coverage. This indicates that a better filtering of high-AOT scenarios is needed in the AVHRR retrieval.

6.2. Surface Assumption

Effective separation of the surface and atmospheric contributions to the radiance observed by a satellite-based sensor at TOA is a key issue in aerosol retrieval. In AVHRR-DB over land, two surface estimation methods have been used depending on the surface types: bright (e.g., barren ground and urban areas) or dark vegetated surfaces (Hsu et al., 2017) as briefly summarized in section 2. Figure 9 shows the AOT difference (AVHRR-DB − CARSNET) as a function of the surface reflectance from the LTDR project as described in section 3.3. In general, the AOT difference increases with increasing surface reflectance, except over very dark surface with a reflectance at 0.63 μm of less than 0.1. For larger values of the surface reflectance at 0.63 μm the AOT difference is around 0.1 but when the surface reflectance exceeds about 0.22, that is, over very bright surfaces, the AOT difference increases fast. This is mainly due to the large AOT underestimation over bright surfaces. The "information content" of the satellite data is reduced with the increase of the surface reflectance and the decoupling of the aerosol and surface contributions to the TOA reflectance becomes more challenging. As a result the AOT uncertainty increases. Figure 10 shows the seasonal pattern of the
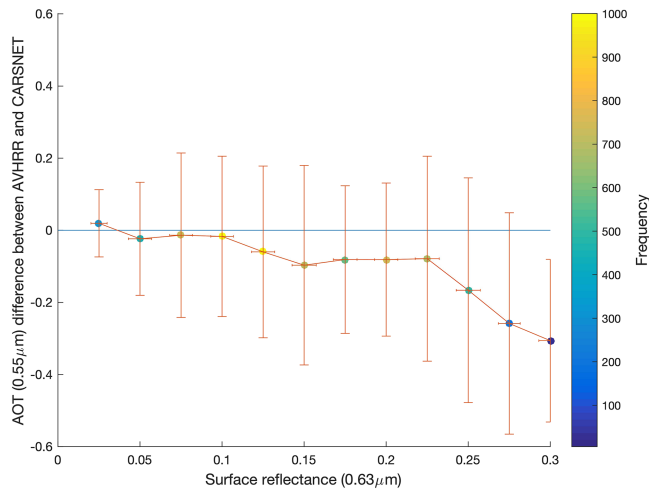
Figure 9. AOT (0.55 μm) difference (AVHRR-DB minus CARSNET) versus surface reflectance at 0.63 μm, where the AOT has been binned in surface reflectance bins with a width of 0.05. Symbols and lines show the mean and standard deviation of the difference between AVHRR and the reference AOT in each bin. Data are only shown for bins with at least five matched data points. The color code indicates the number of match-ups in each bin.

variation of the AOT difference with increasing surface reflectance. The strong gradient for very bright surfaces occurs mainly in the summer and spring, which agrees with previous analysis (de Leeuw et al., 2018). Dust storms in the Taklimakan desert mainly occur in the summer, then in the fall, spring, and winter (Xiao et al., 2008). For surface reflectance at 0.63 μm smaller than 0.125, AVHRR-DB shows very good agreement with CARSNET for all seasons except for the very dark surface in the spring when an unusual "overestimation" is observed. This comes from the dense vegetation sites such as Shangrila, which is located in the southern part of China.

To further investigate the impact of the surface on the retrieval results, a comparison between AVHRR-DB-retrieved AOT and the CARSNET reference AOT over different surface types is presented in Figure 11. The data points in Figure 11 are color coded to indicate the SSA, the effect of which on the retrieval results will be discussed in section 6.4. For all surface types, except mosaic vegetation (50–70%) – cropland (20–50%), more than 300 match-ups are available and the results show the strong dependence of the AVHRR AOT data quality on land cover type. Overall, AVHRR-DB is more accurate and better correlated with CARSNET measurements over vegetated lands (e.g., closed needleleaved evergreen forest, close to open mixed broadleaved and needleleaved forests) and water bodies than over sparse vegetation, Mosaic cropland (50–70%)-vegetation (20–50%) and bare areas. The fractions of the number of data points within EE are around (or more than) 60% for vegetated lands and water bodies, but less than 40% for bare areas. The worst cases are for Mosaic cropland (50–70%)-vegetation (20–50%) and closed to open herbaceous vegetation, with less than 30% (even 20%) of the retrievals within EE. Comparison of the AOT results over Mosaic cropland (50–70%)-vegetation (20–50%)
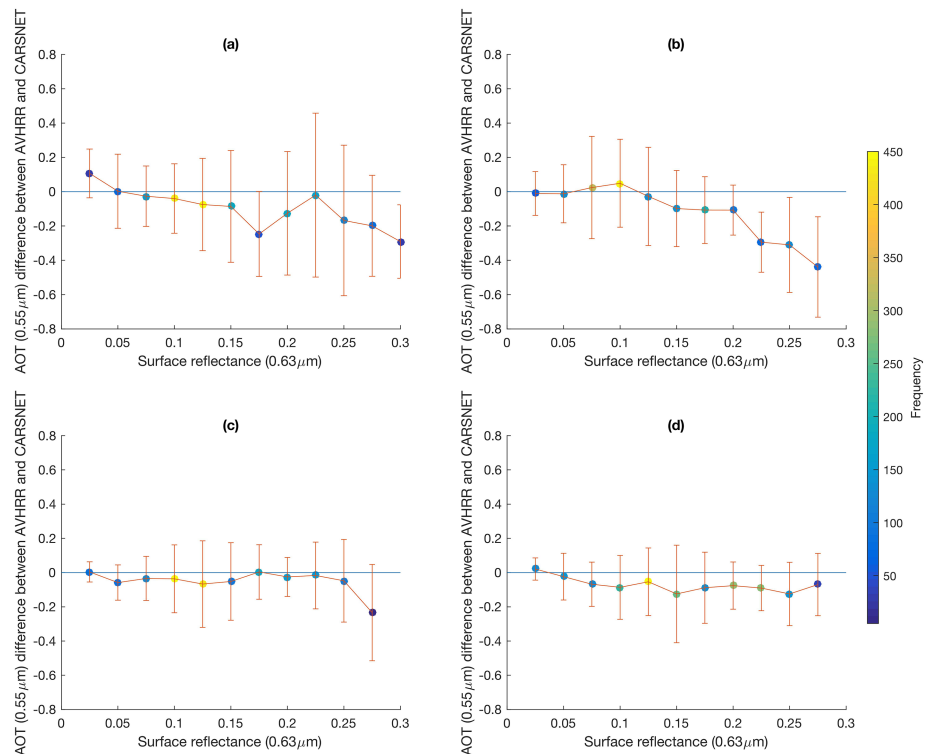
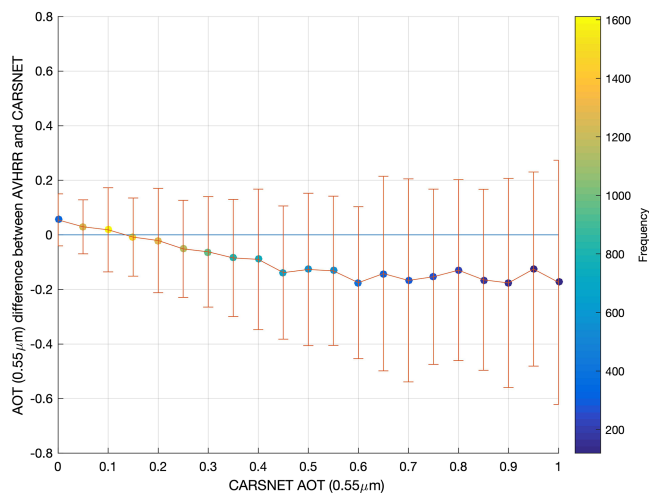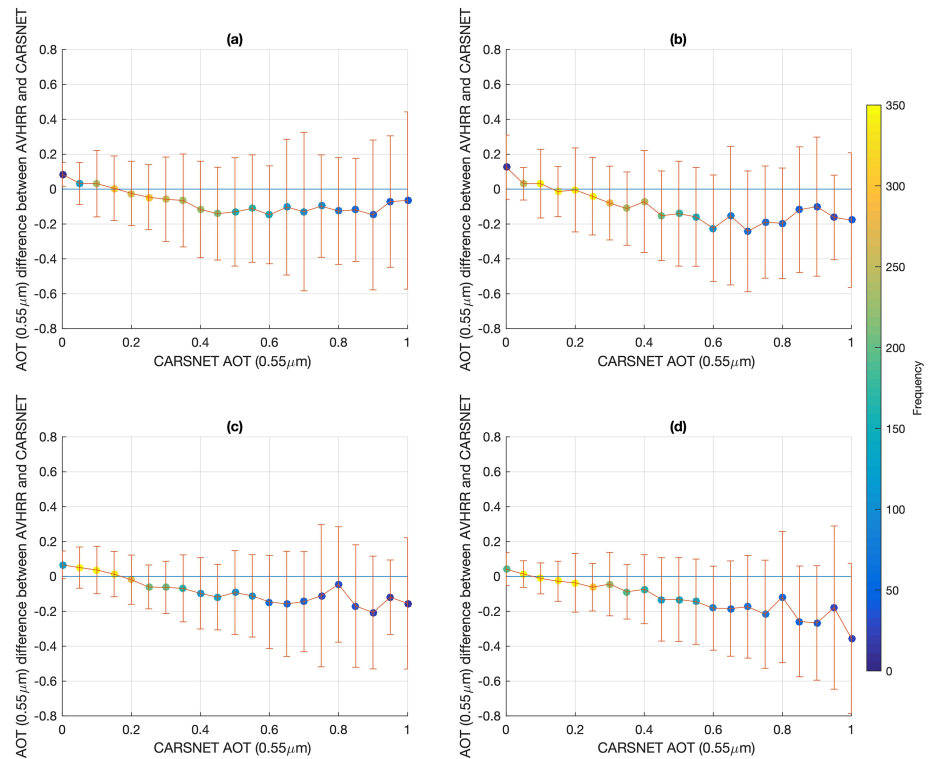**Figure 10.** Same as Figure 9 but for different seasons: (a) MAM, (b) JJA, (c) SON, and (d) DJF.
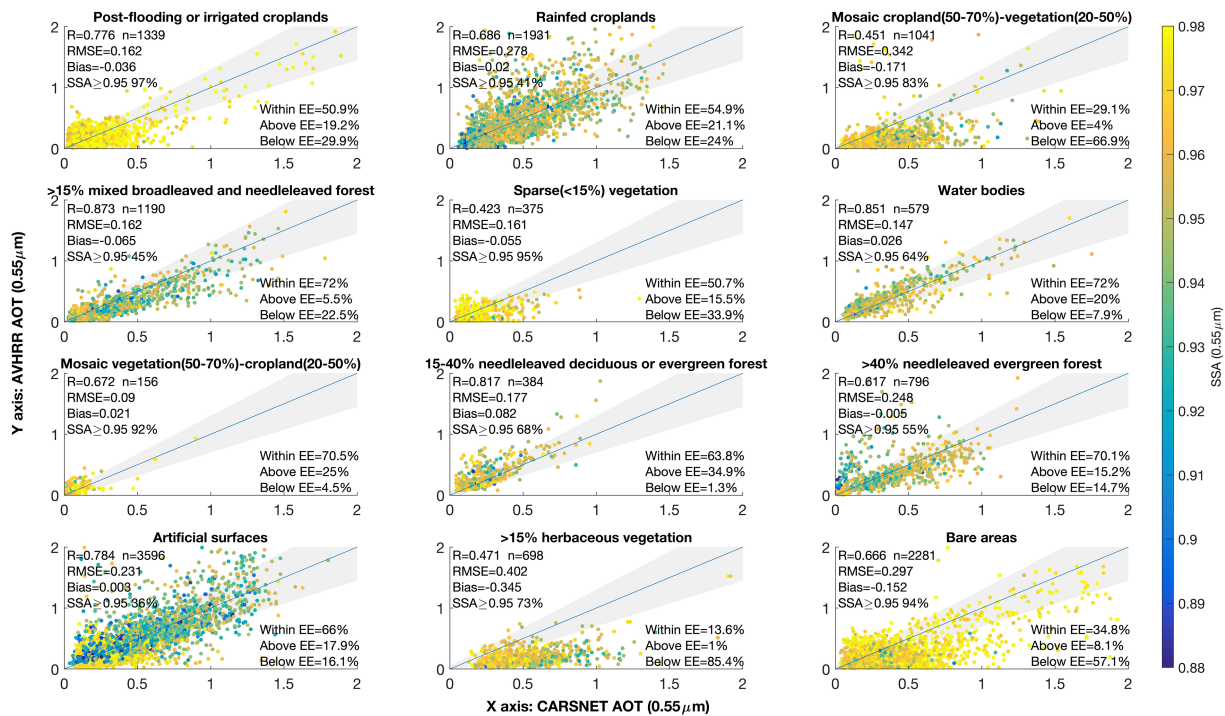
Figure 11. Scatter density plots of AVHRR-DB AOT at 0.55 μm versus CARSNET AOT at 0.55 μm over different land cover types. The identity line is indicated by the blue line and the AVHRR expected error (EE = ± (0.05 + 0.25τ)) is indicated by the shaded gray area. The data points are color coded by the SSA value which is indicated in the color bar at the left. In the top left captions, correlation coefficient (R), number of matchups (n), RMSE, and fraction within EE. In the bottom right captions, statistics binned by AOT intervals.

with those over Mosaic vegetation (50–70%)-cropland (20–50%) shows that the performance is much better over the latter surface type, where the fraction within EE is 70.5% (29.7% for Mosaic cropland (50–70%)-vegetation (20–50%)) and a correlation coefficient of 0.672 (0.451 for Mosaic cropland (50–70%)-vegetation

Figure 12. AOT difference (AVHRR-DB-CARSNET) for AOT at 0.55 μm versus the CARSNET AOT. Here the AOT differences are binned in AOT bins with a width of 0.05 and the data points are color coded to indicate the number of data pints included in the binned sample. The vertical lines indicate the error bars on the 1-sigma uncertainty level.

(20–50%)). This is due to the complicated surface mixture, which may not accurately enough be described by the surface parameterization. AVHRR-DB tends to perform well when the mosaic vegetation dominates. Another problem of aerosol typing may be introduced over cropland due to agricultural biomass burning; the aerosol optical model of strong biomass burning leads to large (systematic underestimation) errors in high-AOT conditions, which agrees with the analysis presented above. For cases with high absorption (blue to green dots in Figure 11), AVHRR-DB performs quite well regardless of surface type, even for artificial surfaces, with a fraction within EE of 66.0%, correlation coefficient of 0.784, and low bias of 0.003. This may be explained by the suitability of the surface parameterization and aerosol model, especially when AOT is large (e.g., AOT > 0.5 as for cases in artificial surfaces) because the surface is relatively less important when AOD is high, or when absorption is high and thus less radiation reaches the surface. The uncertainty due to surface estimation may be mitigated by the strong aerosol information (strong absorption with large AOT reduces the contribution of the surface reflectance to the TOA reflectance because less solar radiation reaches the surface (Zhang et al., 2018)). Large underestimation of the AVHRR-DB AOT is observed for regions where the aerosol absorption is relatively weak, such as postflooding or irrigated croplands and bare areas.

Figure 13. Same as Figure 12 but for different seasons: (a) MAM, (b) JJA, (c) SON, and (d) DJF.

6.3. Aerosol Loading

In addition to the surface parameterization, aerosol loading and aerosol absorption are also important parameters for an accurate aerosol retrieval. The investigation of the aerosol bias in regard to the aerosol loading, as indicated by AOT magnitude, is critical to understand the retrieval algorithm, especially over high aerosol loading regions, such as China. Figure 12 shows the difference between AVHRR-DB and CARSNET AOTs as a function of the CARSNET AOT, where the AVHRR-DB AOT has been binned in AOT bins with a width of 0.05. The AVHRR-DB-retrieved AOT decreases almost monotonically with increasing CARSNET AOT and is negative for CARSNET AOT larger than 0.15. For the largest AOT values (AOT ≥ 0.6) the difference is almost constant with a value of about 0.17. These bias characteristics share similarities with those found in Sayer et al. (2017). Most cases (more than 70%) occur for AOT smaller than 0.3, where AVHRR-DB performs fairly well (difference between AVHRR-DB and CARSNET is less than 0.05). The large error bars (1 standard deviation) indicate the large variability within the AOT bins. The bias in the AOT differences of about 0.17 for AOT ≥0.6 can be explained partly by the number of samples; that is, the number of samples for AOT = 0.8 and 0.95 is less than 150, which is 5 times less than that for AOT = 0.75.

The bias characteristics with respect to AOT for different seasons are presented in Figure 13. The variation in the AOT difference with the reference AOT is similar in the winter and the summer; that is, the bias is increasingly negative with increasing AOT also for AOT larger than 0.6, indicating the impact of the dominating dust aerosol for the validation. Besides the filtering due to limited information content and the use of possibly inappropriate dust optical properties in the retrieval, the extreme conditions (AOT >0.6) which are captured by CARSNET may be missed by AVHRR-DB, as illustrated below using time series for selected CARSNET sites.

Figure 13 shows different bias characteristics for different seasons, which also differ from the total bias characteristics as shown in Figure 12. For all seasons, the AOT bias tends to be small and positive for low AOT while negative biases occur for higher AOT. However, the critical AOT point where the bias changes from positive to negative is different for each season. In summary, AVHRR-DB retrievals agree satisfactorily with CARSNET for AOT smaller than 0.4 while for AOT larger than 0.6 the AOT is on average underestimated by about 0.15–0.2.
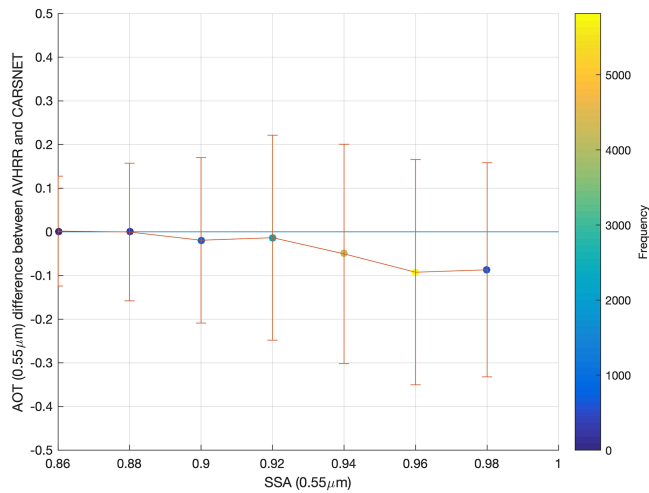
Figure 14. Same as Figure 11 but for SSA at 0.55 μm.

6.4. Aerosol Absorption

Aerosol optical properties, especially aerosol absorption, used to create LUTs, is another key issue for a proper aerosol retrieval, especially for strong aerosol loading episodes such as during dust storms or biomass burning. The effects of aerosol absorption (in terms of SSA) have been indicated in Figure 11, where the AOT over different land cover surface types was color coded according to SSA. Figure 11 shows the combination of the effects of surface type, aerosol loading, and aerosol absorption. The dependence of the AVHRR-DB algorithm purely on aerosol absorption is further evaluated with respect to the binned SSA below. We would like to mention here that the quality of the SSA data set used in this study may play an important role, an updated version of SSA data set with better quality may change the dependence features of AOT uncertainty on SSA, especially when combing different factors together (e.g., AOT, surface type, and aerosol absorption). For example, if absorbing aerosols (determined by SSA) happen to be more frequent at certain CARSNET sites located in regions with more favorable surface conditions in terms of the retrieval performance, the dependence features of AOT uncertainty on SSA may be strongly affected by the surface reflectance. Figure 14 shows the bias characteristics as a function of SSA at 0.55 μm. The distribution of the biases across the SSA range may indicate the dependence of the retrieval accuracy on aerosol absorption. Although the AOT differences between AVHRR-DB and CARSNET increase with increasing SSA (see Figure 14), indicating the better performance of AVHRR-DB for scenarios with high absorption, other factors such as surface reflectance may play a more dominated role here, which can be seen from the seasonal patterns of the AVHRR-DB AOT bias characteristics as shown in Figure 15. All seasons show very different dependences of AOT bias on SSA and no-consistent conclusion can be drawn according to both Figures 14 and 15. An overestimation during spring for strong absorption comes from closed needleleaved evergreen forest surface types, according to RGB visualization, potential cloud
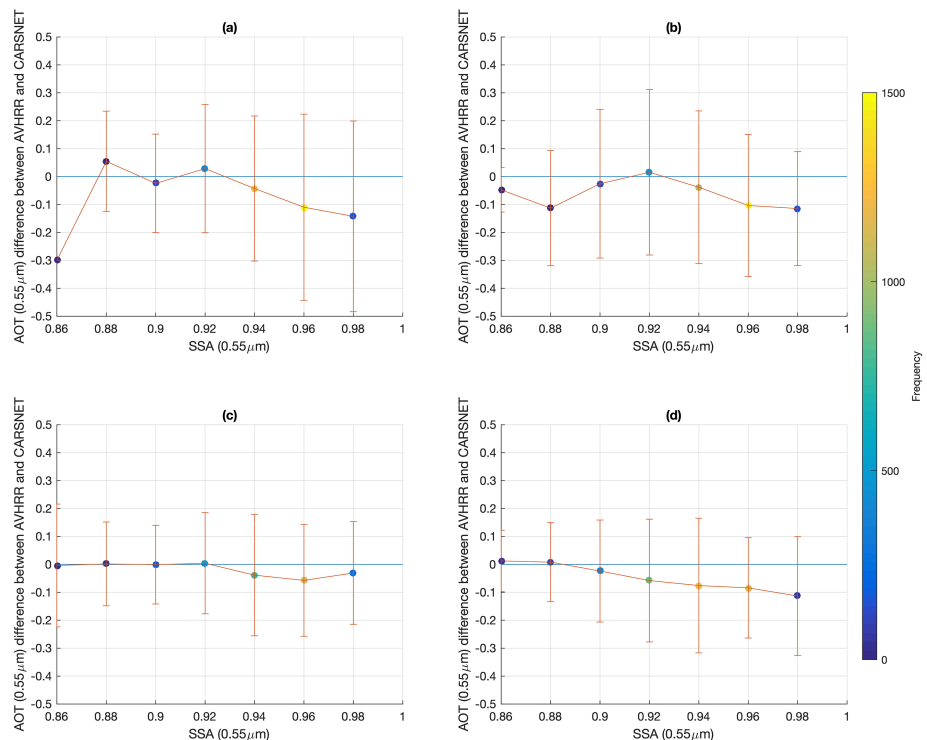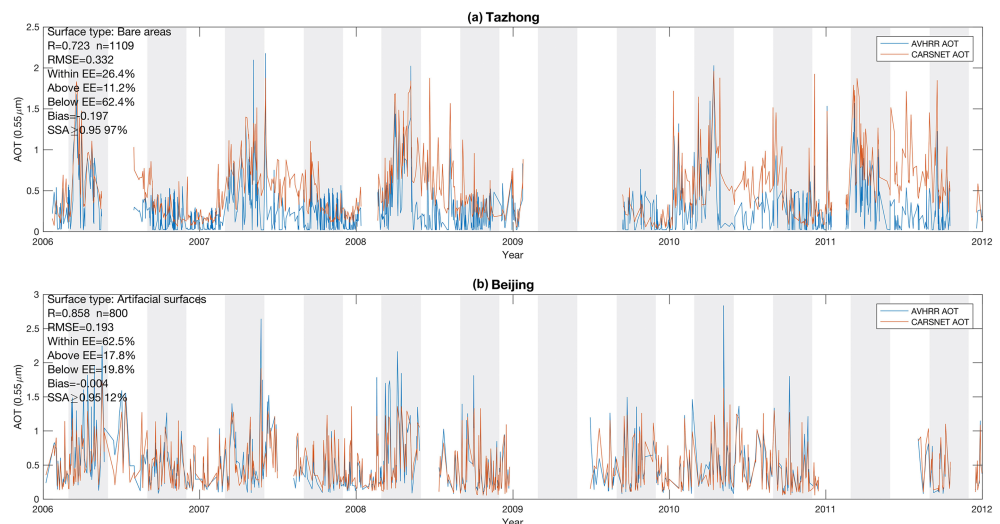

Figure 15. Same as Figure 14 but for different seasons: (a) MAM, (b) JJA, (c) SON, and (d) DJF.

Figure 16. Time series of AOT at 0.55 μm at two CARSNET sites during 2006–2011. The gray area indicates the spring (MAM) and autumn (SON) of each year highlighting the seasonal patterns. Blue and red lines indicate AVHRR and CARSNET AOT.

contamination may contribute to the overestimation of AOT. High absorption occurs both for natural and anthropogenic sources. Natural sources include those over closed needleleaved evergreen forest due to biomass burning. Anthropogenic sources occur over artificial surfaces (such as cities), rainfed croplands, and water bodies due to local or nearby anthropogenic emissions. All have a high fraction of retrieved AOTs within EE, that is, 54.9% over rainfed croplands, 72.0% for closed to open mixed broadleaved and needleleaved forest, 72.0% over water bodies, 70.1% over closed needleleaved evergreen forest, and 66.0% over artificial surfaces. This indicates the strong impacts of surface types on the analysis of the dependence of AOT uncertainties on SSA. Strong aerosol absorption over rainfed cropland mainly occurs during summer time due to agriculture biomass burning. The impact of aerosol absorption plays a more important role for relatively bright surfaces (artificial surfaces) compared to dark surfaces may due to the enhancement of aerosol information content (due to large aerosol loading because larger absorption occurs frequently with large AOT) over bright surfaces, thus easier decoupling of the aerosol and surface contributions to the TOA reflectance. However, potential uncertainties in the SSA data set will also play a role to understand the AVHRR-DB AOT data set quality with respect to aerosol absorbing and we cannot quantify the uncertainties in SSA now.

6.5. Time Series Analysis

All of the above analysis shows the validation from a statistical point of view, this section aims to show the performance of the AVHRR-DB aerosol retrieval algorithm for a single site over a long period of time in order to explore the suitability of the AVHRR-DB AOT data set to create a consistent AOT time series. Figure 16 shows such time series for two representative CARSNET sites: Tazhong (located in the Taklamakan desert region) and Beijing. The time series includes the whole period studied here, that is, 2006–2011. The selected sites are representative for the most complicated cases for aerosol retrieval due to the surface properties (desert and urban) and the variability of aerosol types combined with the occurrence of very high AOTs. At the Tazhong site (Figure 16a), the AOT is underestimated during the whole period of time, especially during the summer. The underestimation of about 0.05 for AOT smaller than 0.6 is mainly caused by the bias due to the surface parameterization, as discussed in section 6.2, and the aerosol typing of AVHRR-DB over the Chinese desert regions, as was previously concluded by Tao et al. (2017). However, for strong dust storm cases (AOT >1), mainly during the summer period, the AVHRR AOT can be a factor of 2 lower than the reference value. The bias with high AOT was discussed in section 6.3, but there only averages were shown including many data points; for individual data pints the bias may be much larger as shown here in Figures 15 and 16. During autumn, the AVHRR AOT may be 2 times higher than the CARSNET reference value which is likely due to cloud contamination. The performance of AVHRR-DB is much better over Beijing. Some

overestimation of AOT during spring time may be due to the problem of misclassification of high AOT situations as cloud, as discussed in section 6.1. The above time series analysis indicates the stability of the AVHRR Deep Blue AOT product.

7. Conclusion

The aim of creating an AVHRR aerosol product is to produce the longest satellite-based global aerosol data record to support aerosol research on both regional and global scales from a long-term perspective. A good understanding of the data quality, especially over areas such as China with a large variety of aerosol types and strong emissions of both natural and anthropogenic aerosols, is urgently needed. In this paper, the recently released AVHRR-DB aerosol product (version 1.0) over land (Hsu et al., 2017; Sayer et al., 2017) has been critically evaluated over China using the CARSNET AOT data set (Che et al., 2015) as reference. This work has been used for a better understanding of the AVHRR aerosol data set over a variety of surfaces and in different aerosol conditions. The global AVHRR-DB AOT product has been validated with AERONET Sun photometer AOT data by Sayer et al. (2017). The current study complements this work with additional information over China, where limited AERONET sites are available but with a good coverage of CARSNET sites across the whole country.

The AVHRR AOT product has been validated using a two-step strategy. The first step is to gain a general understanding of the AVHRR AOT patterns by comparison with the MODIS/Aqua AOT C6.1 product. This comparison shows that the AVHRR-DB AOT over eastern China is lower than the MODIS C6.1 AOT, while over western China the two data sets have similar AOT values, although large differences occur locally. The AOT at both AVHRR wavelengths (0.55 and 0.63 μm) has been validated using CARSNET AOT data and the results have been further linked to key factors affecting aerosol retrieval, including cloud screening and pixel filtering, surface typing/surface reflectance, aerosol loading, and aerosol absorption. The main findings are the following: (1) the overall validation shows that AVHRR-DB AOT is in reasonable agreement with that from MODIS and CARSNET, indicating the successful implementation of the original SeaWiFS/MODIS DB algorithm to AVHRR; (2) the extrapolation of AOT from 0.63 to 0.55 μm using an Ångström exponent climatology works quite well; (3) about 53.8% of the AVHRR-DB AOT data over China fall within the (±0.25AOT ± 0.05) error envelope; (4) AVHRR underestimates the AOT and the underestimation increases almost linearly with the increase of AOT up to AOT = 0.6; (5) AVHRR-DB performs better over relatively dark surfaces (e.g., when the mosaic vegetation dominates) than over bright surfaces, and the overfiltering of strong aerosol loading scenarios such as dust storms suggests that further improvement is needed; and (6) the AOT differences between AVHRR-DB and CARSNET increase over bright surfaces with increasing SSA due to smaller aerosol loading (AOT).

The instrument calibration issue, which has been discussed in Sayer et al. (2017), is not included in this paper. However, both lack of information content and calibration are as important as the factors discussed in this paper. In spite of those two intrinsic properties of AVHRR (lack of information content and calibration issue), the first DB aerosol product has potential for many quantitative scientific applications and may be improved further by refinement of the retrieval algorithm and improved sensor calibration (Sayer et al., 2017).

References

Bontemps, S., Defourny, P., van Bogaert, E., Kalogirou, V., & Arino, O. (2011). GlobCover 2009: Products description and validation report. ESA GlobCover project, 53 pp.

Che, H., Zhang, X., Chen, H., Damiri, B., Goloub, P., Li, Z., et al. (2009). Instrument calibration and aerosol optical depth (AOD) validation of the China Aerosol Remote Sensing Network (CARSNET). *Journal of Geophysical Research*, *114*, D03206. https://doi.org/10.1029/2008JD011030

Che, H., Zhang, X.-Y., Xia, X., Goloub, P., Holben, B., Zhao, H., et al. (2015). Ground-based aerosol climatology of China: aerosol optical depths from the China Aerosol Remote Sensing Network (CARSNET) 2002–2013. *Atmospheric Chemistry and Physics*, *15*, 7619–7652. https://doi.org/10.5194/acp-15-7619-2015

de Leeuw, G., Holzer-Popp, T., Bevan, S., Davies, W., Descloitres, J., Grainger, R. G., et al. (2015). Evaluation of seven European aerosol optical depth retrieval algorithms for climate analysis. *Remote Sensing of Environment*, *162*, 295–315. https://doi.org/10.1016/j.rse.2013.04.023

de Leeuw, G., Sogacheva, L., Rodriguez, E., Kourtidis, K., Georgoulias, A. K., Alexandri, G., et al. (2018). Two decades of satellite observations of AOD over mainland China using ATSR-2, AATSR and MODIS/Terra: data set evaluation and large-scale patterns. *Atmospheric Chemistry and Physics*, *18*(3), 1573–1592. https://doi.org/10.5194/acp-18-1573-2018

Duveiller, G., Hooker, J., & Cescatti, A. (2018). The mark of vegetation change on Earth's surface energy balance. *Nature Communications*, *9*(679).

Fraser, R. S., & Kaufman, Y. J. (1985). The relative importance of scattering and absorption in remote sensing. *IEEE. Transactions on Geoscience and Remote Sensing*, *23*, 625–633. https://doi.org/10.1109/TGRS.1985.289380

Gao, L., Li, J., Chen, L., Zhang, L., & Heidinger, A. K. (2016). Retrieval and validation of atmospheric aerosol optical depth from AVHRR over China. *IEEE Transactions on Geoscience and Remote Sensing*, *54*(11), 6280–6291. https://doi.org/10.1109/TGRS.2016.2574756

Geogdzhayev, I. V., & Mishchenko, M. I. (2015). Validation of Long-Term Global Aerosol Climatology Project Optical Thickness Retrievals Using AERONET and MODIS Data. *Remote Sensing*, *7*, 12,588–12,605. https://doi.org/10.3390/rs71012588

Geogdzhayev, I. V., Mishchenko, M. I., Rossow, W. B., Cairns, B., & Lacis, A. A. (2002). Global two-channel AVHRR retrievals of aerosol properties over the ocean for the period of NOAA-9 observations and preliminary retrievals using NOAA-7 and NOAA-11 data. *Journal of the Atmospheric Sciences*, *59*(3), 262–278. https://doi.org/10.1175/1520-0469(2002)059<0262:GTCARO>2.0.CO;2

Gong, S. L., Zhang, X. Y., Zhao, T. L., McKendry, I. G., Jaffe, D. A., & Lu, N. M. (2003). Characterization of soil dust aerosol in China and its transport and distribution during 2001 ACE-Asia: 2. Model simulation and validation. *Journal of Geophysical Research*, *108*(D9), 4262. https://doi.org/10.1029/2002JD002633

Hansell, R. A., Ou, S. C., Liou, K. N., Roskovensky, J. K., Tsay, S. C., Hsu, C., & Ji, Q. (2007). Simultaneous detection/separation of mineral dust and cirrus clouds using MODIS thermal infrared window data. *Geophysical Research Letters*, *34*, L11808. https://doi.org/10.1029/2007GL029388

Hauser, A., Oesch, D., Foppa, N., & Wunderle, S. (2005). NOAA AVHRR derived aerosol optical depth over land. *Journal of Geophysical Research*, *110*, D08204, 1–11. https://doi.org/10.1029/2004JD005439

Holben, B. N., Eck, T. F., Slutsker, I., Tanre, D., Buis, J. P., Setzer, A., et al. (1998). AERONET – A federated instrument network and data archive for aerosol characterization. *Remote Sensing of Environment*, *66*(1), 1–16. https://doi.org/10.1016/S0034-4257(98)00031-5

Holben, B. N., Kim, J., Sano, I., Mukai, S., Eck, T. F., Giles, D. M., et al. (2018). An overview of mesoscale aerosol processes, comparisons, and validation studies from DRAGON networks. *Atmospheric Chemistry and Physics*, *18*, 655–671. https://doi.org/10.5194/acp-18-655-2018

Hollmann, R., Merchant, C., Saunders, R., Downy, C., Buchwitz, M., Cazenave, A., et al. (2013). The ESA climate change initiative: satellite data records for essential climate variables. *Bulletin of the American Meteorological Society*, *94*, 1541–1552. https://doi.org/10.1175/BAMS-D-11-00254.1

Hsu, N. C., Jeong, M. J., Bettenhausen, C., Sayer, A. M., Hansell, R., Seftor, C. S., et al. (2013). Enhanced Deep Blue aerosol retrieval algorithm: The second generation. *Journal of Geophysical Research: Atmospheres*, *118*, 9296–9315. https://doi.org/10.1002/jgrd.50712

Hsu, N. C., Lee, J., Sayer, A. M., Carletta, N., Chen, S. H., Tucker, C. J., et al. (2017). Retrieving near-global aerosol loading over land and ocean from AVHRR. *Journal of Geophysical Research: Atmospheres*, *122*, 9968–9989. https://doi.org/10.1002/2017JD026932

Hsu, N. C., Tsay, S. C., King, M. D., & Herman, J. R. (2004). Aerosol properties over bright-reflecting source regions. *IEEE Transactions on Geoscience and Remote Sensing*, *42*(3), 557–569. https://doi.org/10.1109/TGRS.2004.824067

Ichoku, C., Chu, D., Mattoo, S., Kaufman, Y. J., Remer, L., Tanre, D., et al. (2002). A spatio-temporal approach for global validation and analysis of MODIS aerosol products. *Geophysical Research Letters*, *29*(12), 1616. https://doi.org/10.1029/2001GL013206

Kaufman, Y. J., Tanre, D., & Boucher, O. (2002). A satellite view of aerosols in the climate system. *Nature*, *419*(6903), 215–223. https://doi.org/10.1038/nature01091

Kaufman, Y. J., Wald, A. E., Remer, L. A., Bo-Cai Gao, Rong-Rong Li, & Flynn, L. (1997). The MODIS 2.1 mm channel—Correlation with visible reflectance for use in remote sensing of aerosol. *IEEE Transactions on Geoscience and Remote Sensing*, *35*(5), 1286–1298. https://doi.org/10.1109/36.628795

Kolmonen, P., Sogacheva, L., Virtanen, T. H., de Leeuw, G., & Kulmala, M. (2016). The ADV/ASV AATSR aerosol retrieval algorithm: current status and presentation of a full-mission AOD data set. *International Journal of Digital Earth*, *9*(6), 545–561. https://doi.org/10.1080/17538947.2015.1111450

Koren, I., Remer, L. A., Kaufman, Y. J., Rudich, Y., & Martins, J. V. (2007). On the twilight zone between clouds and aerosols. *Geophysical Research Letters*, *34*, L08805. https://doi.org/10.1029/2007GL029253

Lacagnina, C., Hasekamp, O. P., Bian, H., Curci, G., Myhre, G., van Noije, T., et al. (2015). Aerosol single-scattering albedo over the global oceans: Comparing PARASOL retrievals with AERONET, OMI, and AeroCom models estimates. *Journal of Geophysical Research: Atmospheres*, *120*, 9814–9836. https://doi.org/10.1002/2015JD023501

Levy, R. C., Mattoo, S., Munchak, L. A., Remer, L. A., Sayer, A. M., Patadia, F., & Hsu, N. C. (2013). The Collection 6 MODIS aerosol products over land and ocean. *Atmospheric Measurement Techniques*, *6*, 2989–3034. https://doi.org/10.5194/amt-6-2989-2013

Levy, R. C., Munchak, L. A., Mattoo, S., Patadia, F., Remer, L. A., & Holz, R. E. (2015). Towards a long-term global aerosol optical depth record: applying a consistent aerosol retrieval algorithm to MODIS and VIIRS-observed reflectance. *Atmospheric Measurement Techniques*, *8*(10), 4083–4110. https://doi.org/10.5194/amt-8-4083-2015

Levy, R. C., Remer, L. A., Kleidman, R. G., Mattoo, S., Ichoku, C., Kahn, R., & Eck, T. F. (2010). Global evaluation of the Collection 5 MODIS dark-target aerosol products over land. *Atmospheric Chemistry and Physics*, *10*, 10,399–10,420. https://doi.org/10.5194/acp-10-10399-2010

Li, Z., Zhao, X., Kahn, R., Mishchenko, M., Remer, L., Lee, K.-H., et al. (2009). Uncertainties in satellite remote sensing of aerosols and impact on monitoring its long-term trend: a review and perspective. *Annals of Geophysics*, *27*(7), 2755–2770. https://doi.org/10.5194/angeo-27-2755-2009

Liu, N., Zou, B., Feng, H., Tang, Y., & Liang, Y. (2019). Evaluation and comparison of MAIAC, DT and DB aerosol products over China, *Atmospheric Chemistry and Physics Discussions*, 1–34. https://doi.org/10.5194/acp-2018-1339

Liu, Q., Ding, W.-D., & Fu, Y.-F. (2011). the Seasonal Variations of Aerosols over East Asia as Jointly Inferred from MODIS and OMI. *Atmospheric and Oceanic Science Letters*, *4*(6), 330–337. https://doi.org/10.1080/16742834.2011.11446952

Martins, J. V., Tanré, D., Remer, L., Kaufman, Y. J., Mattoo, S., & Levy, R. (2002). MODIS Cloud screening for remote sensing of aerosols over oceans using spatial variability. *Geophysical Research Letters*, *29*(12), 1619. https://doi.org/10.1029/2001GL013252

Martins, V. S., Lyapustin, A., Carvalho, L. A. S., Barbosa, C. C. F., & Novo, E. M. L. M. (2017). Validation of high-resolution MAIAC aerosol product over South America. *Journal of Geophysical Research: Atmospheres*, *122*, 7537–7559. https://doi.org/10.1002/2016JD026301

Mei, L., Rozanov, V., Vountas, M., Burrows, J. P., & Richter, A. (2018). XBAER-derived aerosol optical thickness from OLCI/Sentinel-3 observation. *Atmospheric Chemistry and Physics*, *18*, 2511–2523. https://doi.org/10.5194/acp-18-2511-2018

Mei, L., Xue, Y., de Leeuw, G., Holzer-Popp, T., Guang, J., Li, Y., et al. (2012). Retrieval of aerosol optical depth over land based on a time series technique using MSG/SEVIRI data. *Atmospheric Chemistry and Physics*, *12*(19), 9167–9185. https://doi.org/10.5194/acp-12-9167-2012

Mei, L. L., Rozanov, V., Vountas, M., Burrows, J., Levy, R., & Lotz, W. (2017a). Retrieval of aerosol optical properties using MERIS observations: algorithm and some first results. *Remote Sensing of Environment*. https://doi.org/10.1016/j.rse.2016.11.015,197,125-140

Mei, L. L., Rozanov, V., Vountas, M., Burrows, J., Levy, R., & Lotz, W. (2017b). A Cloud masking algorithm for the XBAER aerosol retrieval using MERIS data. *Remote Sensing of Environment*, *197*, 141–160. https://doi.org/10.1016/j.rse.2016.11.016

Mei, L. L., Rozanov, V., Vountas, M., Burrows, J. P., & Richter, A. (2018). XBAER-derived aerosol optical thickness from OLCI/Sentinel-3 observation. *Atmospheric Chemistry and Physics*, *18*, 2511–2523. https://doi.org/10.5194/acp-18-2511-2018

Mei, L. L., Xue, Y., Kokhanovsky, A. A., von Hoyningen-Huene, W., de Leeuw, G., & Burrows, J. P. (2014). Retrieval of aerosol optical depth over land surfaces from AVHRR data. *Atmospheric Measurement Techniques*, *7*, 2411–2420. https://doi.org/10.5194/amt-7-2411-2014

Mei, L. L., Xue, Y., Xu, H., Guang, J., Li, Y. J., Wang, Y., et al. (2012). Validation and analysis of optical thickness retrieval over land. *International Journal of Remote Sensing*, *33*(3), 781–803. https://doi.org/10.1080/01431161.2011.577831

Mishchenko, M. I., Geogdzhayev, I. V., Rossow, W. B., Cairns, B., Carlson, B. E., Lacis, A. A., & Travis, L. D. (2007). Long-term satellite record reveals likely recent aerosol trend. *Science*, *315*(5818), 1543–1543. https://doi.org/10.1126/science.1136709

Popp, T., de Leeuw, G., Bingen, C., Brühl, C., Capelle, V., Chedin, A., et al. (2016). Development, production and evaluation of aerosol Climate Data Records from European satellite observations (Aerosol_cci). *Remote Sensing*, *8*, 421. https://doi.org/10.3390/rs8050421

Proestakis, E., Amiridis, V., Marinou, E., Georgoulias, A. K., Solomos, S., Kazadzis, S., et al. (2018). Nine-year spatial and temporal evolution of desert dust aerosols over South and East Asia as revealed by CALIOP. *Atmospheric Chemistry and Physics*, *18*, 1337–1362. https://doi.org/10.5194/acp-18-1337-2018

Remer, L. A., Tanre, D., Kaufman, Y. J., Ichoku, C., Mattoo, S., Levy, R., et al. (2002). Validation of MODIS aerosol retrieval over ocean. *Geophysical Research Letters*, *29*(11), 8008. https://doi.org/10.1029/2001GL013204

Riffler, M., Popp, C., Hauser, A., Fontana, F., & Wunderle, S. (2010). Validation of a modified AVHRR aerosol optical depth retrieval algorithm over Central Europe. *Atmospheric Measurement Techniques*, *3*, 1255. https://doi.org/10.5194/amt-3-1255-2010

Sayer, A. M., Hsu, N. C., Bettenhausen, C., Ahmad, Z., Holben, B. N., Smirnov, A., et al. (2012). SeaWiFS Ocean Aerosol Retrieval (SOAR): Algorithm, validation, and comparison with other data sets. *Journal of Geophysical Research*, *117*, D03206. https://doi.org/10.1029/2011JD016599

Sayer, A. M., Hsu, N. C., Bettenhausen, C., & Jeong, M.-J. (2013). Validation and uncertainty estimates for MODIS Collection 6 "Deep Blue" aerosol data. *Journal of Geophysical Research: Atmospheres*, *118*, 7864–7872. https://doi.org/10.1002/jgrd.50600

Sayer, A. M., Hsu, N. C., Bettenhausen, C., Jeong, M.-J., & Meister, G. (2015). Effect of MODIS Terra radiometric calibration improvements on Collection 6 Deep Blue aerosol products: Validation and Terra/Aqua consistency. *Journal of Geophysical Research: Atmospheres*, *120*, 12,157–12,174. https://doi.org/10.1002/2015JD023878

Sayer, A. M., Hsu, N. C., Lee, J., Carletta, N., Chen, S.-H., & Smirnov, A. (2017). Evaluation of NASA Deep Blue/SOAR aerosol retrieval algorithms applied to AVHRR measurements. *Journal of Geophysical Research: Atmospheres*, *122*, 9945–9967. https://doi.org/10.1002/2017JD026934

Sayer, A. M., Munchak, L. A., Hsu, N. C., Levy, R. C., Bettenhausen, C., & Jeong, M.-J. (2014). MODIS Collection 6 aerosol products: comparison between aqua's e-deep blue, dark target, and "merged" data sets, and usage recommendations. *Journal of Geophysical Research: Atmospheres*, *119*, 13,965–13,989. https://doi.org/10.1002/2014JD022453

Shi, G. M., Liu, R. L., Wang, D. Y., & Yang, F. M. (2017). Evaluation of the MODIS C6 Aerosol Optical Depth Products over Chongqing, China. *Atmosphere*, *8*, 227. https://doi.org/10.3390/atmos8110227

Shin, S.-K., Tesche, M., Müller, D., & Noh, Y. (2019). Technical note: Absorption aerosol optical depth components from AERONET observations of mixed dust plumes. *Atmospheric Measurement Techniques*, *12*, 607–618. https://doi.org/10.5194/amt-12-607-2019

Sogacheva, L., de Leeuw, G., Rodriguez, E., Kolmonen, P., Georgoulias, A. K., Alexandri, G., et al. (2018). Spatial and seasonal variations of aerosols over China from two decades of multi-satellite observations – Part 1: ATSR (1995–2011) and MODIS C6.1 (2000–2017). *Atmospheric Chemistry and Physics*, *18*, 11,389–11,407. https://doi.org/10.5194/acp-18-11389-2018

Sogacheva, L., Kolmonen, P., Virtanen, T. H., Rodriguez, E., Saponaro, G., & de Leeuw, G. (2017). Post-processing to remove residual clouds from aerosol optical depth retrieved using the Advanced Along Track Scanning Radiometer. *Atmospheric Measurement Techniques*, *10*, 491–505. https://doi.org/10.5194/amt-10-491-2017

Song, Z., Liang, S. L., Wang, D. D., Zhou, Y., & Jia, A. L. (2018). Long-term record of top-of-atmosphere albedo over land generated from AVHRR data. *Remote Sensing of Environment*, *211*, 71–88. https://doi.org/10.1016/j.rse.2018.03.044

Takemata, K., Fukui, H., & Kawata, Y. (2006). Retrieval of aerosol optical thickness over land using NOAA/AVHRR data. *Advances in Space Research*, *38*(10), 2208–2211. https://doi.org/10.1016/j.asr.2006.03.042

Tao, M. H., Chen, L. F., Wang, Z. F., Wang, J., Che, H. Z., Xu, X. G., et al. (2017). Evaluation of MODIS Deep Blue Aerosol Algorithm in Desert Region of East Asia: Ground Validation and Intercomparison. *Journal of Geophysical Research: Atmospheres*, *122*, 10,357–10,368. https://doi.org/10.1002/2017JD026976

Virtanen, T. H., Kolmonen, P., Sogacheva, L., Rodríguez, E., Saponaro, G., & de Leeuw, G. (2018). Collocation mismatch uncertainties in satellite aerosol retrieval validation. *Atmospheric Measurement Techniques*, *11*, 925–938. https://doi.org/10.5194/amt-11-925-2018

Wang, J., Xia, X., Wang, P., & Christopher, S. A. (2004). Diurnal variability of dust aerosol optical thickness and Angstrom expo- ¨ nent over dust source regions in China. *Geophysical Research Letters*, *31*, L08107. https://doi.org/10.1029/2004GL019580

Xiao, F. J., Zhou, C. P., & Liao, Y. M. (2008). Dust storms evolution in Taklimakan Desert and its correlation with climatic parameters. *Journal of Geographical Sciences*, *18*(4), 415–424. https://doi.org/10.1007/s11442-008-0415-8

Xue, Y., He, X., de Leeuw, G., Mei, L., Che, Y., Rippin, W., et al. (2017). Long-time series aerosol optical depth retrieval from AVHRR data over land in North China and Central Europe. *Remote Sensing of Environment*, *198*, 471–489. https://doi.org/10.1016/j.rse.2017.06.036

Zhang, X., Zhang, Q., Hong, C., Zheng, Y., Geng, G., Tong, D., et al. (2018). Enhancement of PM2.5 concentrations by aerosol-meteorology interactions over China. *Journal of Geophysical Research: Atmospheres*, *123*(2), 1179–1194. https://doi.org/10.1002/2017JD027524

Zhao, X. P., Heidinger, A. K., & Walther, A. (2016). Climatology analysis of aerosol effect on marine water cloud from long-term satellite climate data records. *Remote Sensing*, *8*(4), 300. https://doi.org/10.3390/Rs8040300